SIAM J. Applied Dynamical Systems
Vol. 11, No. 1, pp. 350–391

Phase Resetting in an Asymptotically Phaseless System: On the Phase Response of Limit Cycles Verging on a Heteroclinic Orbit*

Kendrick M. Shaw†, Young-Min Park‡, Hillel J. Chiel§, and Peter J. Thomas¶

Abstract. Rhythmic behaviors in neural systems often combine features of limit-cycle dynamics (stability and periodicity) with features of near heteroclinic or near homoclinic cycle dynamics (extended dwell times in localized regions of phase space). Proximity of a limit cycle to one or more saddle equilibria can have a profound effect on the timing of trajectory components and response to both fast and slow perturbations, providing a possible mechanism for adaptive control of rhythmic motions. Reyn ["Generation of limit cycles from separatrix polygons in the phase plane" in *Geometrical Approaches to Differential Equations*, Lecture Notes in Math. 810, Springer, New York, 1980, pp. 264–289] showed that for a planar dynamical system with a stable heteroclinic cycle (or separatrix polygon), small perturbations satisfying a net inflow condition will generically give rise to a stable limit cycle (see also [J. Guckenheimer and P. Holmes, *Nonlinear Oscillations, Dynamical Systems, and Bifurcations of Vector Fields*, 3rd ed., Appl. Math. Sci. 42, Springer-Verlag, Berlin, 1990]). Here we consider the asymptotic behavior of the infinitesimal phase response curve (iPRC) for examples of two systems satisfying Reyn's inflow criterion, (i) a smooth system with a chain of four hyperbolic saddle points and (ii) a piecewise linear system corresponding to local linearization of the smooth system about its saddle points. For system (ii), we obtain exact expressions for the limit cycle and the iPRC as functions of a parameter $\mu > 0$ representing the distance from a heteroclinic bifurcation point. In the $\mu \to 0$ limit, we find that perturbations parallel to the unstable eigenvector direction in a piecewise linear region lead to divergent phase response, as previously observed [E. Brown, J. Moehlis, and P. Holmes, *Neural Comput.*, 16 (2004), pp. 673–715]. In contrast to previous work, we find that perturbations parallel to the *stable* eigenvector direction can lead to either divergent or convergent phase response, depending on the phase at which the perturbation occurs. In the smooth system (i), we show numerical evidence of qualitatively similar phase specific sensitivity to perturbation. Having the exact expression for the iPRC for the piecewise linear system allows us to investigate its stability under diffusive coupling. In addition, we qualitatively compare iPRCs obtained for systems (i) and (ii) to iPRCs for the Morris–Lecar equations near a bifurcation from limit cycles to a saddle-homoclinic orbit.

Key words. homoclinic orbit, heteroclinic orbit, phase resetting curve, stable heteroclinic channel, limit cycle, piecewise linear dynamical system, bifurcation, computational neuroscience, central pattern generator

AMS subject classifications. 34C05, 37C27, 37C29, 37G15, 70K05, 70K44

*Received by the editors March 29, 2011; accepted for publication (in revised form) by C. Chow October 24, 2011; published electronically March 13, 2012. This work was supported by National Science Foundation grants DMS-0720142 and DMS-1010434.

http://www.siam.org/journals/siads/11-1/82897.html

†Department of Biology and Medical Scientist Training Program, Case Western Reserve University, 10900 Euclid Avenue, Cleveland, OH 44106 (kms15@case.edu).

‡Department of Mathematics, Case Western Reserve University, 10900 Euclid Avenue, Cleveland, OH 44106 (yxp30@case.edu).

§Departments of Biology, Biomedical Engineering, and Neurosciences, Case Western Reserve University, 10900 Euclid Avenue, Cleveland, OH 44106 (hjc@case.edu).

¶Departments of Biology, Mathematics, and Cognitive Science, Case Western Reserve University, 10900 Euclid Avenue, Cleveland, OH 44106 (pjthomas@case.edu). The work of this author was partially supported by National Science Foundation grant DMS 0931642.

DOI. 10.1137/110828976

1. Introduction. Animals often generate specific sequences of behavior, such as the movements of the limbs during walking, the feeding apparatus while chewing and swallowing, or body undulations in swimming. When a repeated sequence of motions can be produced reliably, the pattern generator circuit controlling the behavior is typically modeled as an autonomous system of ordinary differential equations admitting a stable isolated periodic orbit, i.e., a limit-cycle oscillator [34, 74]. Limit-cycle oscillators have played a fundamental role in understanding the generation and control of repetitive motions underlying swimming in the lamprey [13, 16]; neural activity and bursting [18, 35]; the gaits of quadrupeds [14, 31], bipeds [46], and monopeds [9, 15]; as well as cardiac and respiratory activity [20, 55, 56].

Another class of systems generating reproducible sequences of activity has been proposed under the rubric of *stable heteroclinic sequences* [5] or *stable heteroclinic channels* [49]. A dynamical system possesses a heteroclinic sequence if there exists a chain of hyperbolic saddle fixed points for which the unstable manifold of each saddle intersects the stable manifold of the next [2]; they generalize the notion of a stable heteroclinic cycle, an attractor comprising a finite collection of saddle points with heteroclinic connections linking them in a repeating chain [7, 32, 63, 64]. A heteroclinic cycle is *stable* or *attracting* when the product around the cycle of the saddle values $\{V_i\}$ is strictly greater than unity [4]; the saddle value for a hyperbolic saddle point with eigenvalues $\lambda_u > 0 > \lambda_s^1 \geq \lambda_s^2 \geq \cdots \geq \lambda_s^{n-1}$ is the ratio $-\lambda_s^1/\lambda_u$. We let V_i denote the saddle value for the ith saddle. Stable heteroclinic sequences and cycles have been proposed to provide a framework within nonlinear dynamics for understanding a range of phenomena, including olfactory processing in insects [48], search behavior in the marine mollusk *Clione limacina* [73], "winnerless competition" in neural circuits [1, 4] and ecological models [2], genesis of network-dependent bursting activity [45], and the balance of emotion and cognition in behavioral control [3] as well as other areas [50].

Because they require the intersection of one dimensional unstable and codimension one stable manifolds, the saddle connections comprising a heteroclinic cycle are structurally unstable [6]. For planar systems, Reyn showed that a phase portrait containing a separatrix polygon generically forms a limit cycle when subject to a perturbation satisfying a net inflow condition [53], provided that the unperturbed heteroclinic cycle is attracting. Trajectories near an unperturbed attracting heteroclinic cycle traverse the cycle with longer and longer return times; the trajectory along the heteroclinic cycle itself has "infinite period." Similarly, for limit cycles arising from perturbations satisfying the net inflow condition, the smaller the size of the perturbation, the longer the period of the limit cycle.

As an example, consider the system defined on the 2-torus $0 \leq y_i \leq 2\pi$, $i \in \{1, 2\}$:

$$\frac{dy_1}{dt} = f(y_1, y_2) = \cos(y_1)\sin(y_2) + \alpha\sin(2y_1), \tag{1.1a}$$

$$\frac{dy_2}{dt} = g(y_1, y_2) = -\sin(y_1)\cos(y_2) + \alpha\sin(2y_2). \tag{1.1b}$$

As shown in Figure 1(a), this system has four saddle points connected by heteroclinic connections. The saddles have identical eigenvalues $\lambda_u = 1 - 2\alpha$, $\lambda_s = -1 - 2\alpha$, so the product of

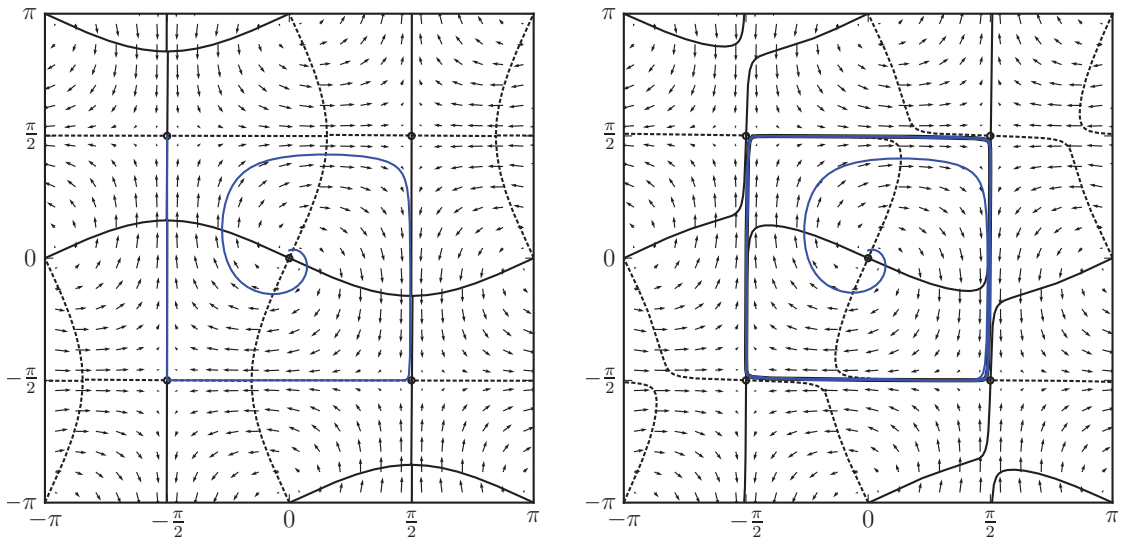

Figure 1. *Parametric perturbation of an attracting heteroclinic cycle to a stable limit cycle. The solid line is the x-nullcline, and dashed is the y-nullcline.* (a) *A trajectory of the smooth toroidal system given by* (1.1)*, passing near four distinct saddles each with eigenvalues* $\lambda_s = -1 - 2\alpha$ *and* $\lambda_u = 1 - 2\alpha$*. The trajectory shown begins near the unstable spiral point at location* (π, π) *near the center of the plot. The trajectory was integrated for a total time of* 200 *units using* $\alpha = 7/30$ *and* $\mu = 0$*. It passes closer to each successive saddle, slowing progressively.* (b) *The perturbed system* (1.2) *when* $\alpha = 7/30$ *and* $\mu = 0.01$ *forms a stable limit cycle passing close to the four saddle points. Please see the corresponding movie* 82897_01.mpg [local/web 6.13MB]*; this animation cycles through phase portraits for the smooth system for values of* μ *varying from* 0 *to* 1/2 *and back again. At* $\mu = 2\alpha$ *the limit cycle collapses via a Hopf bifurcation to a single stable fixed point located between the four surrounding saddles.*

the saddle values, $V = \prod_{i=1}^{4} V_i$, is $V = (\frac{1+2\alpha}{1-2\alpha})^4$. If $\alpha \in (0, 1/2)$, then $V > 1$, indicating that the heteroclinic 4-cycle is attracting.

Although the heteroclinic cycle connecting the four saddle points is structurally unstable, any perturbation of the vector field that pushes the unstable manifold of each saddle towards the interior of the cycle relative to the stable manifold of the next saddle will generically lead to the formation of a stable limit cycle. For example, consider the effects of "rotation" of the flow of equations (1.1) parametrized by $1 > \mu > 0$:

$$\frac{dy_1}{dt} = f(y_1, y_2) + \mu g(y_1, y_2), \tag{1.2a}$$

$$\frac{dy_2}{dt} = g(y_1, y_2) - \mu f(y_1, y_2). \tag{1.2a}$$

We will refer to this system as the *smooth system*, in contrast to the piecewise linear system to be introduced subsequently. As shown in Figure 1(b), for $\mu > 0$ the heteroclinic connections are broken, but a limit cycle has been created inside of the saddles that passes near each of the saddle points.

For any small positive value of μ, system (1.2) will have a stable limit cycle, $\gamma(t) = \gamma(t+T)$, with period $T(\mu) \to \infty$ as $\mu \to 0^+$. For $\mu > 0$ we may identify a phase $\theta \in [0, \theta_{\max})$ with

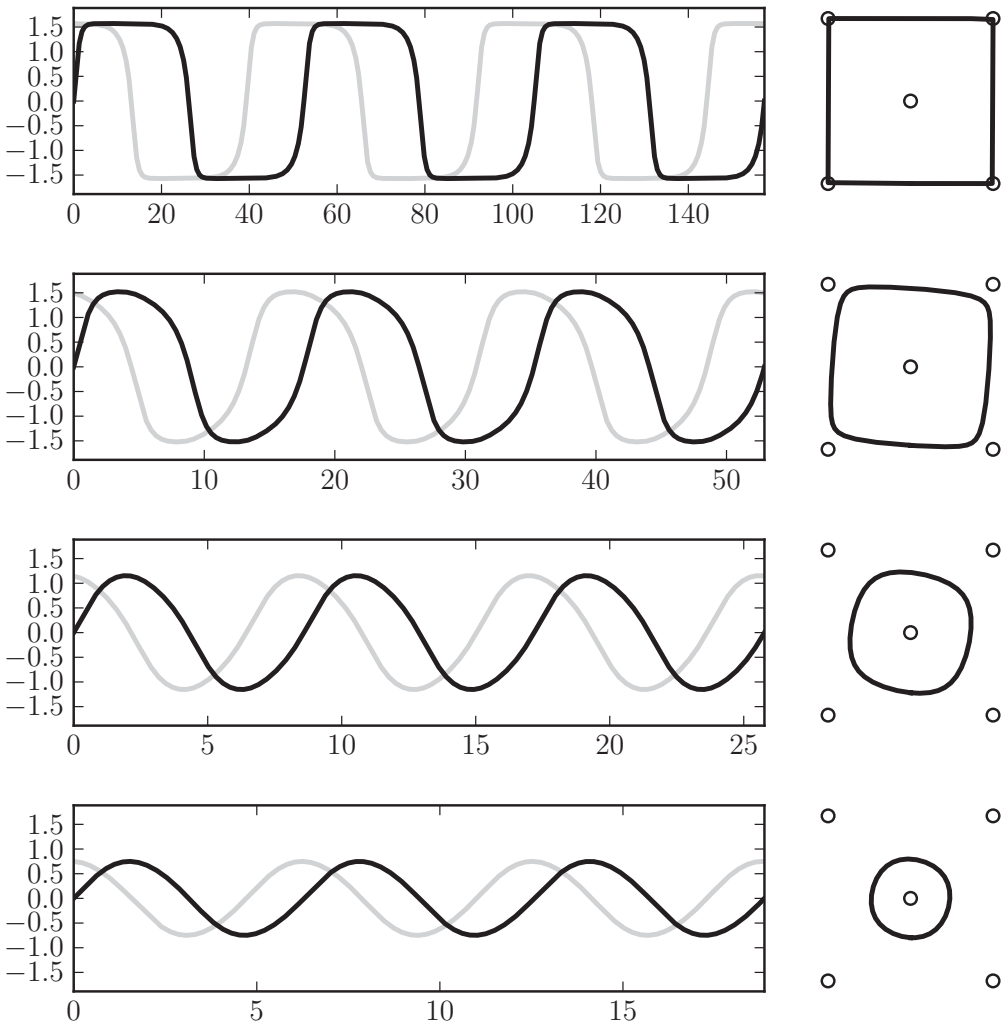

Figure 2. *Time plots of limit cycle trajectories of the smooth system with various values of μ. When $\mu \ll 1$ the time plots exhibit prolonged dwell times due to slow transits past the saddle points and relatively rapid transits between them. As μ increases, the limit cycle moves away from the saddle points, and the speed becomes more uniform (note the change in horizontal scale). As a result, the time plots become more sinusoidal, resembling an Andronov–Hopf oscillator. The first and second ordinates are shown in black and gray, respectively, with $\alpha = 7/30$. From top to bottom $\mu = 10^{-3}, 0.1, 0.3, 0.45$. Compare Figure 5.*

each point on the limit cycle by choosing an arbitrary point γ_0 to have phase $\theta(\gamma_0) = 0$ and requiring $d\theta/dt = \theta_{\max}/T(\mu)$. Typically one chooses $\theta_{\max}$ to equal either 2π or unity. Because of the fourfold symmetry of the systems considered here it will be convenient to set $\theta_{\max} = 4$ throughout, so that traversal of each quarter of the limit cycle will correspond to a unit increment in phase. Figure 2 illustrates the time course of trajectories of equations (1.2) for $\alpha = 7/30$ and $\mu \in \{10^{-3}, 0.1, 0.3, 0.45\}$.

To each point $\xi_0 = (x_0, y_0)$ in the basin of attraction of the limit cycle we may assign

an asymptotic phase $\phi(\xi_0) \in [0, 4)$ satisfying $||\xi(t) - \gamma(t - \theta(\xi_0)T/4)|| \to 0$ as $t \to \infty$, where $\xi(t)$ and $\gamma(t)$ are solutions of (1.2) satisfying initial conditions $\xi(0) = \xi_0$ and $\gamma(0) = \gamma_0$, respectively, and $||(x, y)|| = |x| + |y|$. The level curves of ϕ, called isochrons, foliate the basin of attraction; see [35] for examples.

An important question for understanding the dynamics of control in central pattern generators (CPGs) is how such systems combine robustness to perturbation with flexibility to adapt behavior to variable environmental or physiological conditions.[1] Many biological systems combining repetitive behavior and behavioral or metabolic control exhibit limit-cycle behavior that is strongly influenced by passage of trajectories near one or more unstable fixed points or quasi equilibria. A recent model for the generation of multiple rhythmic states in a respiratory CPG [55] provides an example. This model examined dynamic reconfiguration of a CPG network by external inputs as a mechanism for adaptive alteration of patterned rhythmic output. During normal rhythmic activity, trajectories of the system decomposed into a series of slowly varying components separated by rapid switching, for instance from an expiratory to an inspiratory phase of activity. Control of the rhythm through changes in the period as well as the duration of different functional phases could be effected by modulatory signals making small changes to the dynamics of escape and release from inhibition, thereby changing the paths of trajectories in the vicinity of quasi equilibria. Similarly, control of the net speed of motion produced by a model locomotory CPG coupled to an explicit musculoskeletal system resulted from the adjustment of CPG trajectories in proximity to unstable fixed points of the model [40, 59, 60]. Patterns of biting, swallowing, and rejection in *Aplysia* may be understood in terms of sequential traversals between neuromechanical equilibrium points [65, 66]. During normal cell growth and proliferation a living cell passes repeatedly through several phases (including cell division), yet the cell "cycle" is typically described not as a standard limit cycle but as a sequence of traversals between quasi equilibria that act as checkpoints [70].[2] In the vicinity of each quasi equilibrium, the cell cycle dynamics slow for an indefinite period of time, until a regulating condition is met [44]. In each of these examples, although the flow, strictly speaking, forms a deterministic limit cycle, the behavior may be actively managed through the introduction of *variable dwell times* that function as control points along trajectories.

Families of limit cycles verging on a heteroclinic (or homoclinic) cycle such as the limit cycles of the one parameter family of systems given by (1.2) provide an opportunity for studying the role of saddle points in the control of timing of rhythmic behaviors. As a first step, it is natural to consider the structure of the infinitesimal phase resetting curves which reflect the sensitivity of the return time along the limit cycle to small instantaneous perturbations. When $\mu = 0$ the flow of (1.2) does not admit a periodic solution with finite

[1] Whether originating endogenously (neural noise, internal control mechanisms) or exogenously (environmental fluctuations), perturbations of the system's dynamics occur on a variety of time scales. For clarity we will limit discussion to two extremes of fast and slow perturbations. Perturbations occurring on slow time scales relative to other system dynamics will be referred to below as *static* or *parametric* perturbations, for example fixing a value $\mu > 0$ in (1.2). Fast perturbations will be approximated as instantaneous trajectory dislocations.

[2] Strictly speaking, the system may be viewed as a limit cycle if the dynamics are embedded in a larger space encompassing the control variables as well; the point remains that the periodic behavior is strongly influenced by passage near unstable equilibria or near-equilibria, which function to regulate the timing of the system.

period; consequently the asymptotic phase and hence the phase response is not well defined. However, for any $\mu > 0$ we can define the phase response, and we can study its behavior as the family of limit cycles approaches the heteroclinic cycle.

To fix terminology, for $1 \gg \mu > 0$, consider a trajectory $\xi(t)$ following a stable limit cycle $\gamma : t \in [0, T) \to \gamma(t) \in \mathbb{R}^n$. Suppose that the trajectory is perturbed by a small instantaneous displacement, taking $x(t^-) = \gamma(t + \theta_0 T/4)$ to $x(t^+) = \gamma(t + \theta_0 T/4) + \vec{r}$. Provided that the new initial condition $x(t^+)$ remains within the basin of attraction of the limit cycle, the orbit will approach the limit cycle with $||x(t) - \gamma((t + \theta_1 T/4) \bmod T)|| \to 0$ as $t \to \infty$, for some new phase $\theta_1 \in [0, 4)$, resulting in a shift in asymptotic phase equal to $(\theta_1 - \theta_0) \bmod 4$. The limit cycle's sensitivity to weak instantaneous perturbations typically varies both with the phase at which the perturbation occurs, $\theta_0(t) = 4((t/T) \bmod 1)$, and with the direction in which it occurs, $\eta = \vec{r}/||\vec{r}|| \in \mathbb{R}^n$. Differences in sensitivity at different phases, which are important for understanding possible control mechanisms, are captured by the *infinitesimal phase response curve* or *iPRC*, defined as

$$Z(\theta, \mu, \eta) = \lim_{\epsilon \to 0} \frac{(\theta - \phi(\gamma(\theta T/4) + \epsilon\eta)) \bmod 4}{\epsilon}. \tag{1.3}$$

As above, $\phi(\xi)$ is the asymptotic phase associated with a point ξ in the basin of attraction for the limit cycle, θ is the phase at which the instantaneous perturbation is applied, μ is the parameter controlling proximity to the heteroclinic, η is the direction of the fast perturbation, γ is the limit cycle trajectory and T is its period; the latter two entities are functions of μ. In order to study the behavior of the phase response as the system approaches the heteroclinic configuration, it is important to emphasize that the limit defining the iPRC in (1.3) is taken *before* the subsequent limit $\mu \to 0$.

Analytic calculation of the iPRC is typically accomplished via an adjoint equation method, and exact solutions are known in very few cases [26, 35]. In order to perform the analysis required to gain qualitative insight into the behavior of the phase response under the sequential limits $\epsilon \to 0$, $\mu \to 0$, we construct a piecewise linear approximation to the smooth system. The *iris system*, described below, is topologically equivalent on an open set including the family of limit cycles and the saddle points, and it qualitatively captures the behavior of the smooth system. For the iris system we obtain exact results including the form of the limit cycle for positive μ and an explicit formula for the iPRC. Our main result, stated in Theorem 1 below, shows that for the iris system the sensitivity to small displacements *parallel to the direction of the stable manifold* has two regions with distinct sensitivity behavior. In the limit, as the family of orbits approaches the heteroclinic orbit, there is an interval of phases $\varphi \in [0, \varphi_c]$ for which the infinitesimal phase response goes to zero. This interval is separated by a critical phase φ_c from a second interval $\varphi \in (\varphi_c, 1]$ for which the iPRC diverges to $+\infty$. The junction $\varphi \equiv 0 \pmod 1$ corresponds to the boundary between regions on which we define a piecewise linear dynamics. We show numerically that qualitatively similar results hold for the smooth system.[3]

Limit cycles in piecewise linear (PWL) dynamical systems have been studied previously in several contexts. For instance, in the context of Glass networks [22, 29, 30], PWL systems have

[3]See also section 8.3 for numerically computed iPRCs for the Morris–Lecar system near a bifurcation from a family of limit cycles to a homoclinic orbit.

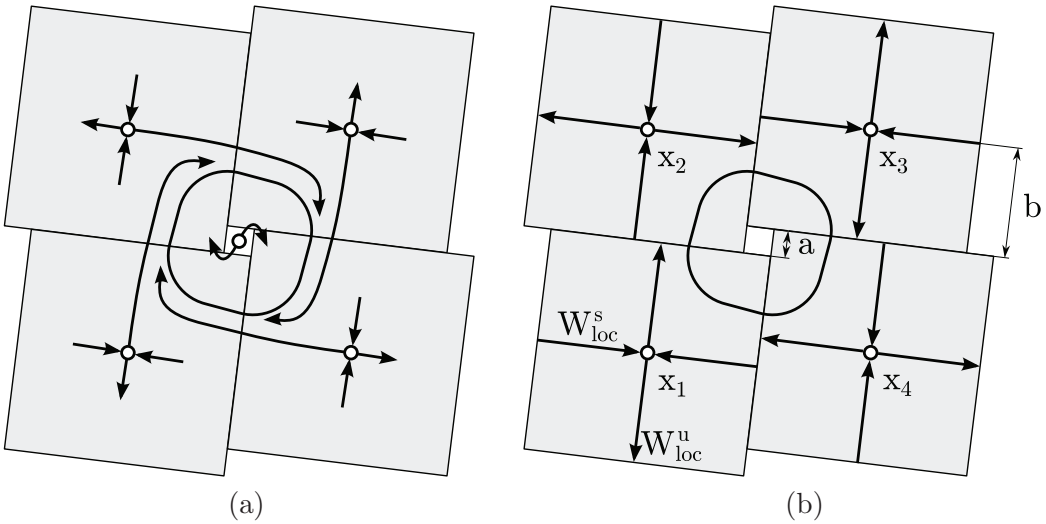

Figure 3. *Construction of the iris system from the smooth system.* (a) *The flow near each saddle point of the smooth system* (1.2) *is approximately linear in a square region aligned with the (orthogonal) eigenvectors. By virtue of the fourfold symmetry of the system, we can extend each square until it has a side of length* 2*b, remaining centered on the saddle. Depending on the extent of the rotational (parametric) perturbation of the vector field, there will be square of side a forming a gap around the unstable spiral point.* (b) *We extend the linearized flow for each saddle throughout the corresponding square of side* 2*b, creating a PWL vector field defined on the plane with the squares of side a removed. The ith square is centered on the ith saddle,* x_i *(*$i = 1, 2, 3, 4$*). In each square the inward arrows indicate* W^s_{loc}*, and the outward arrows indicate* W^u_{loc}*, parallel to the stable and unstable eigenvector directions, respectively.*

been used to represent the dynamics of idealized genetic regulatory systems. In this case, the structure is somewhat different from that considered here, in that the fixed point driving the flow in each PWL region is strictly attracting and lies outside the region, rather than having one unstable eigendirection and lying inside the corresponding flow region. Consequently, families of limit cycles verging on a heteroclinic cycle do not appear in Glass networks. PWL planar dynamical systems in which a fixed point and a limit cycle coexist do occur in models approximating the FitzHugh–Nagumo equations; such systems were used to study traveling wave phenomena [41] and period adding bifurcations under periodic forcing [19]. Neither homoclinic nor heteroclinic cycles appear in these systems, however. Recently, Coombes investigated phase response curves for limit cycles in both the PWL McKean–Nagumo model and a new model related to the Morris–Lecar system [17]; this paper exploited the existence of exact solutions for the iPRC to study synchronization in gap-junction coupled networks, in both the strong and weak coupling limits. The PWL Morris–Lecar system does contain a homoclinic bifurcation; to the best of our knowledge, however, the analysis presented here is the first to obtain exact results for the scaling of the iPRC as a system of limit cycles approaches a saddle-homoclinic or heteroclinic orbit.

2. The PWL iris system.

As $\mu \to 0^+$, the period of the limit cycle in system (1.2) diverges, and the asymptotic phase may no longer be defined. Nevertheless, the response of the system to small, transient perturbations remains of interest. To explore behavior analogous to phase resetting in the $\mu \to 0^+$ limit, we introduce a PWL planar dynamical system analogous to the

smooth system in (1.1). Figure 3(a) illustrates the construction: we tile the plane with large squares of size $2b$ centered on each saddle, and smaller squares of size a between them. When the rotation parameter μ is zero, the large squares align, and the square of side a vanishes. As the vector field "rotates" in the vicinity of each saddle, the squares rotate, and a increases from zero. Within each square, we introduce coordinates $\xi = (s, u)$. With respect to these coordinates, the local flow obeys the linear equations

$$ds/dt = -\lambda s, \tag{2.1}$$

$$du/dt = u. \tag{2.2}$$

Here $\lambda > 0$ is the eigenvalue corresponding to the eigenvector $(1, 0)$ tangent to the stable manifold $W^s_{loc} = \{(s, 0) | -b < s < b\}$. The unstable manifold $W^u = \{(0, u) | -b < u < b\}$ is tangent to the eigenvector $(0, 1)$ corresponding to the unstable eigenvalue, which without loss of generality is set to 1. The stable and unstable eigenvectors are arranged so that when $a > 0$ the flow on the inner quadrants of each square moves clockwise; the flow leaving the square around the ith saddle enters the square around the $i + 1$st saddle (mod 4), as shown in Figure 3.

Formally, for $k \in \{1, 2, 3, 4\}$ let the center of the kth square, (x_k, y_k), be given by the real and imaginary parts, respectively, of $z_k = \sqrt{2}(-i)^k(be^{-i\pi/4} + (a/2)e^{i\pi/4})$, where $0 \le a < b$. Define the kth square to be $S_k = \{(x, y) : |x - x_k| \le b \ \& \ |y - y_k| \le b\}$. In the interior of the first square, the flow satisfies $\dot{x} = -\lambda(x - x_1)$ and $\dot{y} = y - y_1$. The flow in the interior of squares two through four is defined so that the vector field is equivariant with respect to fourfold rotation about the origin. Adjacent squares form a boundary of length $(2b - a)$. At the boundary between S_k and S_{k+1}, the flow leaves S_k and enters S_{k+1}, by construction. The vector field is discontinuous across these boundaries. For definiteness, we take the flow at points on the mutual boundary $S_k \cap S_{k+1}$ of adjacent squares to be defined so that the vector field is continuous when approached from square S_{k+1}, the square into which the trajectories enter.[4]

The four offset squares may be repeated to form a partial tiling of the plane, leaving a complementary set composed of smaller squares of size a. We will view the entire system as confined to the 2-torus, however. We leave the flow unspecified in the interiors of the small squares, and we take any egress points from a large square into a small square to be absorbing; i.e., the flow is set to zero at the boundary of the small squares. Since we are interested in the phase response of limit cycles whose basins of attraction are entirely contained within the larger squares, the flow in the smaller squares is of no consequence. Figure 4 illustrates the system and shows sample trajectories for different values of a. We will refer to the PWL system as the *iris system* because it resembles the iris of a camera, opening and closing as a increases or decreases.

It is clear that the iris system will form a stable heteroclinic orbit when $a = 0$ (corresponding to $\mu = 0$ in the smooth system); we will show in section 3.2 that it also exhibits

[4]Formally, the piecewise linear flow defined here is an example of a *differential inclusion* [11, 27, 39]. In our case, the component of the flow transverse to a domain boundary does not change sign across the mutual edge of adjacent boxes; therefore the technical machinery of differential inclusion theory is not needed to specify the flow unambiguously.

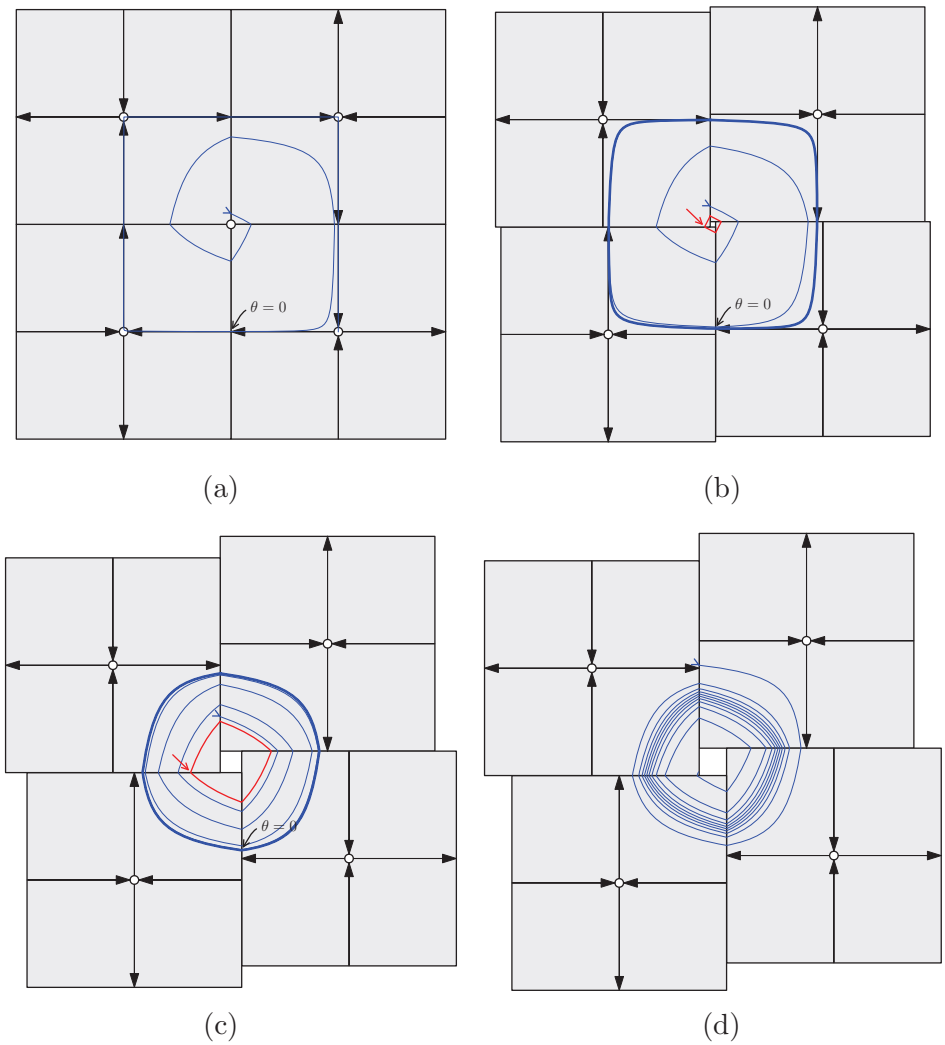

Figure 4. *The behavior of the iris system depends on the offset a. The system is shown rotated through an angle of $-\tan^{-1}(a/b)$ for easier visual comparison with the smooth system.* (a) $a = 0$. *When the offset a is* 0*, the unstable manifold of each saddle connects to the stable manifold of the next, forming a stable heteroclinic orbit. (Thin blue line: sample trajectory. All trajectories proceed clockwise.)* (b) $a = 0.05$. *When $0 < a \ll 1$, a stable limit cycle exists that passes close to the saddles. Its basin of attraction extends inward to a small, unstable limit cycle around the center (red curve and arrow).* (c) $a = 0.2$. *As a increases, the limit cycle becomes more rounded and the flow along the limit cycle more regular.* (d) $a = 0.255$. *If a continues to grow, the stable and unstable limit cycles disappear in a fold bifurcation. Please see the corresponding movie* 82897_02.mpg [local/web 5.90MB]*; this animation cycles through phase portraits of the iris system for values of a ranging from* 0 *to* 0.255 *and back again.*

stable limit cycles passing near the saddles for small values of $a > 0$ (corresponding to $\mu > 0$), as shown in Figure 4. When the limit cycle exists, as above, we assign a phase θ to each point γ in the cycle as the fraction of the cycle's period (scaled by $\theta_{\max} = 4$) required to reach that

point from a defined starting point $\gamma(0) = \gamma_0$ on the cycle, i.e.,

$$\theta(\nu) = \frac{4}{T} \min\big(\{t > 0 \mid \gamma(t) = \nu\}\big), \tag{2.3}$$

where T is the period, i.e., $T = \min(\{t > 0 \mid \gamma(t) = \gamma_0\})$. It is clear that, with this transformation, $d\theta/dt$ is constant and equal to $4/T$. We define the point where the limit cycle first enters the bottom left square (surrounding saddle S_1) as γ_0.

Because the flow is PWL, we may derive analytically the form of the phase response curve for any values of $\lambda > 1 > a > 0$ for which a stable limit cycle exists.

Theorem 1. *Let $\lambda > 1 > a > 0$, let the iris system be defined as in section 2, and define the function*

$$\rho(u) = u^\lambda - u + a. \tag{2.4}$$

1. *If the function ρ has two isolated positive real roots, then the iris system has a stable limit cycle. Let u denote the smallest positive real root of (2.4). The limit cycle trajectory enters each square at local coordinates $(1, u)$ and exits each square at local coordinates $(s, 1)$, where $s = u^\lambda$. The period of the limit cycle is $T = 4\log(1/u)$.*
2. *Let $\theta \in [0, 4)$ be the phase of an instantaneous perturbation in direction η, and let $\theta = k + \varphi$, where $\varphi \in [0, 1)$ and $k \in \{0, 1, 2, 3\}$. If $k = 0$, then the infinitesimal phase response of the limit cycle is*

$$Z(\eta, \varphi, a) = \frac{\eta \cdot \beta(\varphi)}{\log(1/u)(u - \lambda s)}, \tag{2.5}$$

   where $\beta(\varphi) = (s^{(1-\varphi)}, u^\varphi)$ and $\eta = (\eta_s, \eta_u)$ is a unit vector in the L_1 norm. If $k \in \{1, 2, 3\}$, then the infinitesimal phase response is given by $Z(\eta', \varphi, a)$, where $\eta' = \mathcal{R}^k \eta$ and $\mathcal{R} = \left(\begin{smallmatrix} 0 & -1 \\ 1 & 0 \end{smallmatrix}\right)$. The magnitudes of the phase responses to perturbations parallel to the stable and unstable eigenvector directions is greatest at phases corresponding to boundaries between PWL regions.
3. *As $a \to 0$ for fixed λ, the entry coordinate scales as $u = a + o(a)$, the infinitesimal phase response to perturbations parallel to the unstable eigendirection in a given square diverges, and the response to perturbations parallel to the stable eigendirection diverges when $\varphi \in (1 - 1/\lambda, 1)$; otherwise, it converges to zero.*

Figure 5 illustrates the time course of trajectories of the iris system for $\lambda = 2$ and $a \in \{10^{-3}, 0.1, 0.2, 0.24\}$.

While a general consideration of phase resetting in the vicinity of a heteroclinic bifurcation on an invariant circle (or, similarly, near a homoclinic bifurcation) is beyond the scope of this paper, it is natural to conjecture that the limiting behavior of phase response curves near such bifurcations may be similar to that observed here. We discuss the form analogous results might take in a higher dimensional setting in section 8.5.

Lemmas 3 and 4 in section 3 provide necessary and sufficient conditions to guarantee the existence of a stable limit cycle. Lemmas 6, 7, and 8 in section 4 develop the response of a limit-cycle trajectory to a small transient perturbation, leading to direct calculation of the iPRC. Lemmas 10 and 11 in section 5 describe the asymptotic behavior of the iris system in

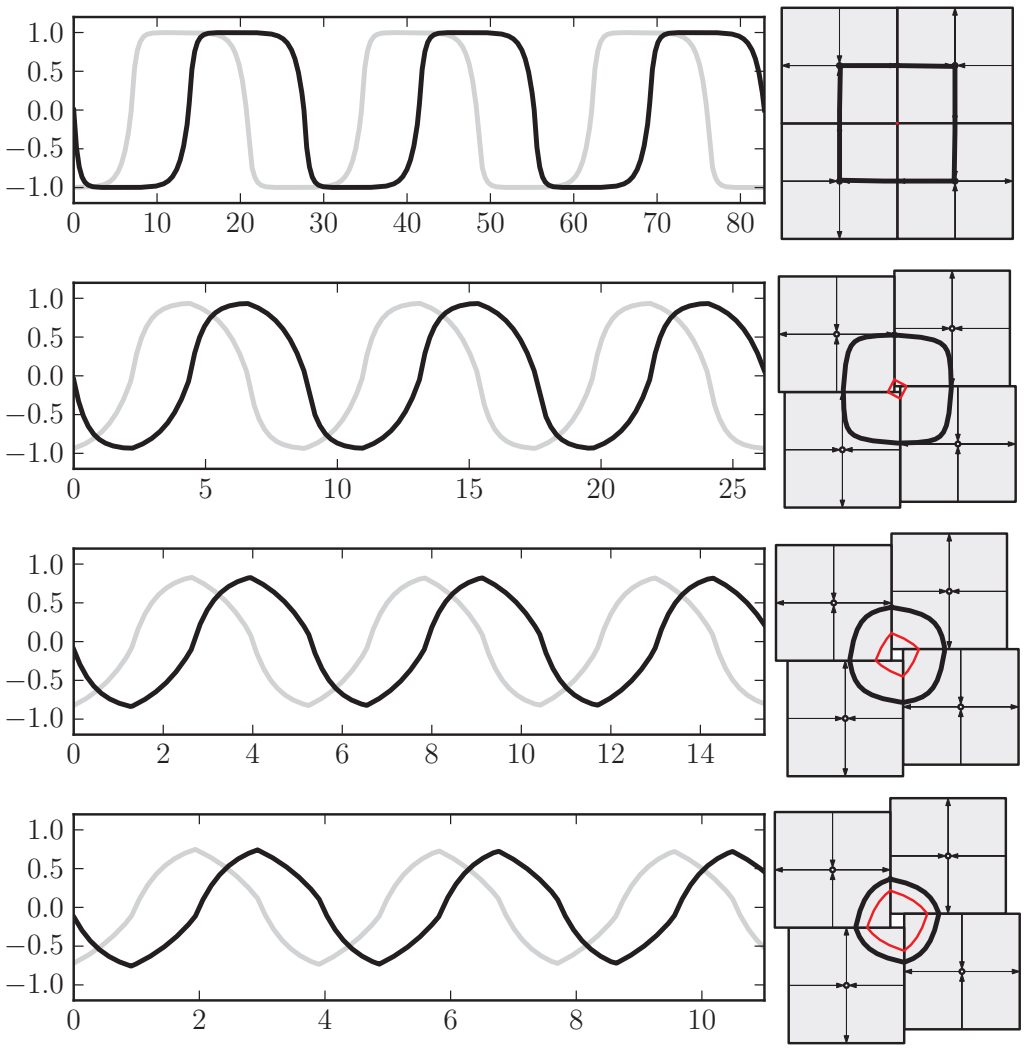

Figure 5. *Time plots of limit cycle trajectories of the iris system with various values of a. When $a \ll 1$ the trajectories slow dramatically when passing near the saddles and travel more quickly between them, resulting in time plots with prolonged dwell times. As a increases, the limit cycle moves away from the saddle points, and the limit cycle trajectory becomes faster and more uniform in speed, resulting in time plots with a more sinusoidal character (note the change in horizontal scale). The horizontal and vertical ordinates are shown in black and gray, respectively, with $\lambda = 2$. From top to bottom $a = 10^{-3}, 0.1, 0.2, 0.24$. Compare Figure 2.*

the heteroclinic limit, i.e., as $a \to 0$. In section 5 we also compare analytic and numerical results for the phase response curves of the iris system. In section 6 we numerically explore the isochrons of the iris system. In section 7 we numerically obtain phase response curves for the smooth system given by (1.1) and compare their structure with those of the iris system. In order to make a qualitative comparison between our results and a system enjoying direct biological motivation, in section 8.3 we show iPRCs obtained numerically for the planar Morris–Lecar system near a bifurcation from a family of limit cycles to a saddle homoclinic

orbit. In section 8.4 we confirm numerically and analytically that the iPRCs obtained for our PWL iris system successfully predict the stability of the synchronous solution for pairs of identical iris systems with diffusive coupling.

In [12] Brown, Moehlis, and Holmes studied phase response curves for limit cycles near the four codimension one bifurcations leading to periodic firing in standard neuronal models (saddle-node bifurcation of fixed points on a periodic orbit, supercritical Hopf bifurcation, saddle-node bifurcation of limit cycles, and homoclinic bifurcation). Their analysis of the homoclinic bifurcation corresponds to our analysis of the iris system in a certain limit; for a detailed comparison, see section 8.2.

3. Limit cycles in the iris system.

We now prove several results about the PWL iris system that we will need to prove Theorem 1. We start by studying the trajectory within one of the square regions to construct a map from the time and position of entry into the region to the time and position of egress out of the region. Next, we connect four of the linearized regions together. We then prove the existence of a limit cycle for sufficiently small values of $a > 0$. We also examine the effects of a perturbation of the trajectory within the neighborhood on the exit time and exit position. We use the maps thus derived to show that a stable limit cycle exists, and use the perturbation results to determine the asymptotic effect of a small perturbation on the phase of the oscillator (i.e., the phase response curve). First, we will examine the dynamics within a single linear region around a saddle of the iris system.

Remark 2 (nondimensionalization). *Assume that each saddle of the iris system has two real orthogonal eigenvectors, one stable and one unstable. Assume that the region around each saddle is a square aligned with these vectors and centered on the saddle with a length of $2L$ along each side (so that the saddle is a distance of L away from each edge). We will refer to the unstable eigenvalue of the saddle as $\lambda_u > 0$ and the stable eigenvalue as $\lambda_s < 0$. The trajectories within the region have the dynamics*

$$\frac{ds}{dt} = \lambda_s s, \qquad \frac{du}{dt} = \lambda_u u. \tag{3.1}$$

Assume that when a trajectory leaves the edge of one region at position $x_f = (s_f, u_f) = (s_f, L)$, it enters the next region with an offset of a, i.e., $x_i = (s_i, u_i) = (L, s_f + a)$. (See the construction in Figure 3.) We assume that there is a cycle of four regions which the trajectory may traverse this way.

We can nondimensionalize the system by defining the new state variables $s^* = s/L$ and $u^* = u/L$, by rescaling time as $t^* = \lambda_u t$ and the offset as $a^* = a/L$. We may define $\lambda = -\lambda_s/\lambda_u$ as the saddle ratio, which will play a critical role in stability (section 3.2). Using these definitions, the governing equations become

$$\frac{ds^*}{dt^*} = -\lambda s^*, \qquad \frac{du^*}{dt^*} = u^*. \tag{3.2}$$

We will use the nondimensionalized version of the system for the remainder of the paper. For simplicity of notation, we will omit the asterisks in what follows.

3.1. Dynamics within a linear region.

Within a single square region surrounding a given saddle point, we will use the local coordinates (s, u) to represent the displacement parallel to

the stable and unstable eigenvectors, respectively. The line segments $\{(s,0) \in \mathbb{R}^2 | 0 \le s \le 1\}$ and $\{(0,u) \in \mathbb{R}^2 | 0 \le u \le 1\}$ are part of the stable and unstable manifolds of the saddle, respectively, forming separatrices of the flow in the square. We will restrict attention to flow entering the square along the edge $\{(1,u) \in \mathbb{R}^2 | 0 < u < 1\}$. It is easy to see that a trajectory entering at an initial point $x_i \equiv (s_i, u_i) = (1, u_i)$ at time t_i with $u_i > 0$ will exit at point $(s_f, u_f) = (s_f, 1) = (u_i^\lambda, 1)$ at time $\log(1/u_i)$. We define the map $f_l : \mathbb{R} \to \mathbb{R}$ from an entry position along the $s = 1$ edge to an exit position along the $u = 1$ edge of the region of linear flow, and a function $T_1(u_i)$ representing the transit time from an entry position $(1, u_i)$:

$$f_l(u_i) = u_i^\lambda, \qquad T_1(u_i) = \log(1/u_i). \tag{3.3}$$

Note that f_l is a monotonically increasing function of u_i and that T_1 is a monotonically decreasing function of u_i.

The closest approach of a trajectory to the saddle point occurs when the position $x = (s, u)$ is perpendicular to the velocity $v = (-\lambda s, u)$, or $0 = -\lambda \exp[-2\lambda t] + u_i^2 \exp[2t]$. Similarly, one may calculate the time at which the speed of the trajectory is minimal. These times are

$$t_{\text{closest}} = \frac{\log\lambda - 2\log u_i}{2(\lambda+1)}, \qquad t_{\text{slowest}} = \frac{3\log\lambda - 2\log u_i}{2(\lambda+1)}. \tag{3.4}$$

We can examine the position of closest approach by integrating the system from the entry position for a time t_{closest}, which gives the location

$$u_{\text{closest}} = u_i e^{t_{\text{closest}}} = u_i \left(\lambda/u_i^2\right)^{1/(2\lambda+2)},$$
$$s_{\text{closest}} = e^{-\lambda t_{\text{closest}}} = \left(u_i^2/\lambda\right)^{\lambda/(2\lambda+2)}.$$

Taking the ratio of the two coordinates, we find

$$u_{\text{closest}} = \lambda^{1/2}\ s_{\text{closest}}, \tag{3.5}$$

and thus the point of closest approach of each trajectory in this quadrant lies along a line passing through the saddle. A similar calculation using t_{slowest} shows that the slowest points lie along the line

$$u_{\text{slowest}} = \lambda^{3/2}\ s_{\text{slowest}}, \tag{3.6}$$

which also passes through the saddle point at the origin of the local coordinate system.

3.2. Dynamics across regions. We will next explore the conditions under which the iris system contains a limit cycle.

Lemma 3. *The iris system described in section 2 contains a limit cycle iff the function*

$$\rho(u) = u^\lambda - u + a$$

has isolated real roots $u^\dagger, u^\ddagger \in (0,1)$, with $u^\dagger \le u^\ddagger$. These roots exist iff $\lambda > 1$ and

$$\lambda^{\lambda/(1-\lambda)} - \lambda^{1/(1-\lambda)} + a \le 0.$$

Proof. To track crossings between regions, we will add a subscript to the variable names indicating how many region crossings have occurred since time $t = 0$, so that $u_{i,3}$ is the ingress location (u_i) immediately after the third crossing.

When $a > 0$, trajectories leaving one region enter the next with an offset a, i.e., ($s_{i,n+1}$, $u_{i,n+1}$) $= (1, s_{f,n} + a)$. We therefore have a second monotonically increasing map from the point of egress along the edge of one square to the entry point along the edge of the next square, $f_e : s_{f,n} \to u_{i,n+1} = s_{f,n} + a$.

We can now form a map from the entry position along the edge of one linear region to the entry position along the edge of the next region via the composition

$$h(u_i) = (f_e \circ f_l)(u_i) = (u_i)^\lambda + a. \tag{3.7}$$

As the composition of two monotonically increasing maps, h is also monotonically increasing. Noting that the entry edges form a transversal section of the flow, it is clear that h^4, the fourfold composition of h, forms a Poincaré map for any cycles crossing this edge. Limit cycles will form isolated fixed points in this map, so to find potential limit cycles we look for points where $u_i = h^4(u_i)$. Because h is composed of four identical monotonic maps, the limit cycles will also be fixed points in these component maps, and thus we have a fixed point at $u_i = u$ iff $u = h(u) = u^\lambda + a$ or, equivalently, $\rho(u) \equiv u^\lambda - u + a = 0$ (cf. (2.4)).

We now consider the potential values of λ, which by definition must be positive. First, consider $0 < \lambda < 1$. Rewriting $\rho(u)$ as $u^\lambda(1 - u^{1-\lambda}) + a$ and remembering that $u \in (0, 1)$, we can see that $\rho(u)$ is now the sum of a positive product and a nonnegative parameter and thus cannot be zero. Next, consider $\lambda = 1$. In this case $\rho(u)$ becomes just a, and thus $\rho = 0$ implies $a = 0$. Note that ρ is independent of u, and thus every $u \in (0, 1)$ is a solution corresponding to a one parameter family of neutrally stable, nonisolated orbits. Therefore λ must be greater than one if a limit cycle exists.

Differentiating ρ twice with respect to u, we find that ρ is convex for all $u > 0$ when $\lambda > 1$, and differentiating it once, we find that ρ has a minimum at

$$(u_i)_{\min} = \lambda^{1/(1-\lambda)}. \tag{3.8}$$

Because $\rho(u)$ is continuous and equal to a when $u = 0$ or $u = 1$, by the midpoint theorem it will have a root between 0 and $(u_i)_{\min}$ and a root between $(u_i)_{\min}$ and 1 iff

$$0 \geq \rho((u_i)_{\min}) = (u_i)_{\min}^\lambda - (u_i)_{\min} + a = \lambda^{\lambda/(1-\lambda)} - \lambda^{1/(1-\lambda)} + a. \tag{3.9}$$

We will call the smaller root $u^\dagger$ and the larger (possibly identical) root $u^\ddagger$. ■

Figure 6 illustrates the map $h = f_e \circ f_l$ when $\lambda = 2$ and $a = 0.2$.

We now examine the stability of the roots $u^\dagger$ and $u^\ddagger$.

Lemma 4. *If the roots $u^\dagger$ and $u^\ddagger$ of (2.4) exist and are distinct, $u^\dagger$ gives the entry position of a stable limit cycle along the $s = 1$ edge of a region, and $u^\ddagger$ gives the entry position of an unstable limit cycle along the same edge.*

Proof. We can determine the stability of the two points by examining the derivative of h at these points; if $|dh/du_i| > 1$, the fixed point will be unstable, and if $|dh/du_i| < 1$, the point will be stable. Because the existence of the roots implies $\lambda > 1$, we know $dh/du_i = (u_i)^{\lambda-1}\lambda$

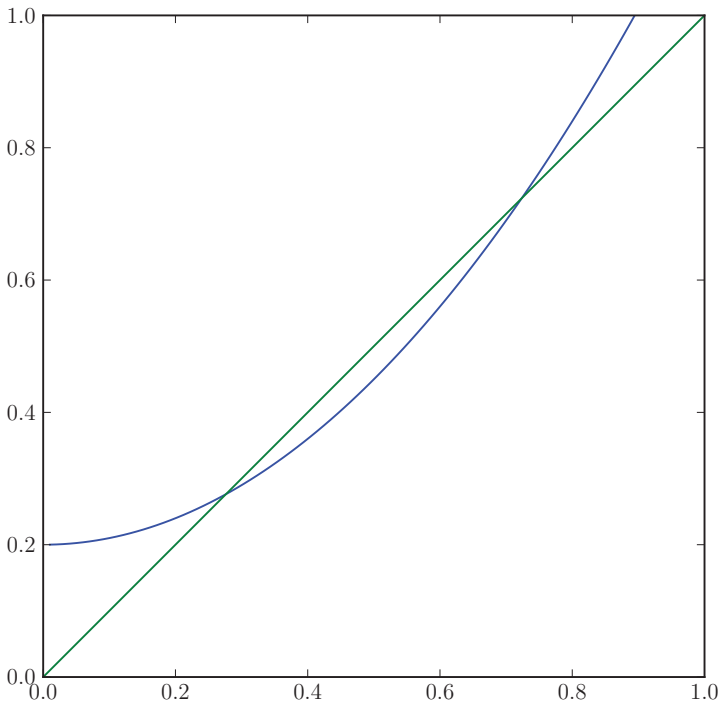

Figure 6. *The map $h = f_e \circ f_l$ from the entry position of a trajectory along the edge of a square to its entry position along the edge of the next square forms a map analogous to a return map (blue curve). This map is continuous and monotonically increasing, so a limit cycle can exist only where a trajectory enters the next square at the same position it entered the current square (green line indicates the identity map). In this example there are two intersections corresponding to the stable and unstable limit cycles. Here $a = 0.2$ and $\lambda = 2$. The blue curve meets the vertical axis at the offset between squares a, and changing the offset raises or lowers the blue curve without changing its shape. Varying a allows for 0, 2, or 1 limit cycles (corresponding to Figure 4(d), Figure 4(c), and the fold bifurcation that occurs between them).*

will be positive. Differentiating h a second time, we see that $d^2h/du_i^2 = (u_i)^{\lambda-2}(\lambda-1)\lambda$ is always greater than zero, and thus dh/du_i is monotonically increasing. Since a fixed point in a map is stable iff the magnitude of the derivative at that point is greater than one, we find the point where dh/du_i passes through 1:

$$1 = dh/du_i = \lambda(u_i)^{\lambda-1}$$

or

$$u_i = \lambda^{1/(1-\lambda)}.$$

This, however, is just $(u_i)_{\min}$ from (3.8). Because this lies between the two roots, $dh/du_i|_{u^\dagger} < dh/du_i|_{(u_i)_{\min}} = 1$, and thus $u^\dagger$ is a stable fixed point of h, and $1 = dh/du_i|_{(u_i)_{\min}} < dh/du_i|_{u^\ddagger}$, and thus $u^\ddagger$ is an unstable fixed point of h. Because h is a Poincaré map at the entry plane of the region, these fixed points correspond to the entry points of a stable and unstable limit cycle, respectively. ■

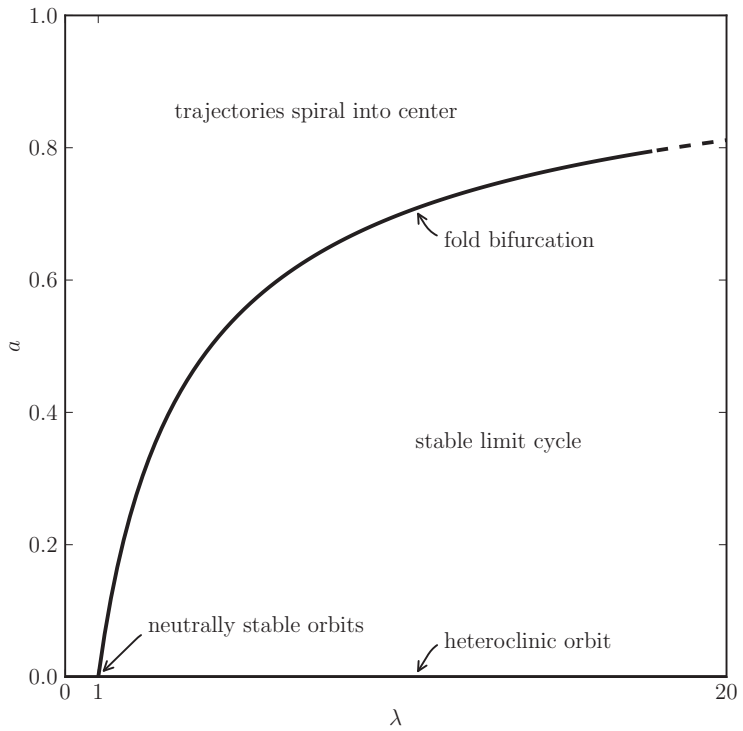

Figure 7. *Two parameter bifurcation diagram for the iris system. When the stable-to-unstable eigenvalue ratio λ is sufficiently large relative to a, a stable and an unstable limit cycle coexist (region labeled "stable limit cycle"). As a increases, the two limit cycles are destroyed in a fold bifurcation (line labeled "fold bifurcation"). As a approaches 0, the system approaches a heteroclinic orbit (line labeled "heteroclinic orbit"). When a is sufficiently large or $\lambda < 1$, trajectories spiral into the center as shown in Figure 4(d) (area labeled "trajectories spiral into center"). When $\lambda = 1$ and $a = 0$, the system becomes a square filled with neutrally stable orbits (point labeled "neutrally stable orbits").*

Remark 5. *Lemmas 3 and 4 together establish Theorem 1, part* 1.

As just shown, for small positive a two limit cycles exist—one stable and one unstable. As $a \to 0$, the stable limit cycle is destroyed in a heteroclinic bifurcation, and the unstable limit cycle collapses to a point at the center of the system. As a increases, the two limit cycles collide in a cycle-cycle fold bifurcation. The collision occurs when the inequality (3.9) becomes an equality. The two roots converge to $(u_i)_{\min}$ as the two limit cycles that cross the section at the two roots merge. Figure 7 shows the bifurcation diagram.

4. Effects of a small instantaneous perturbation.

We now examine the effects of a small perturbation of a trajectory starting on the limit cycle. We will first explore the effects on the exit time and exit position from the square, and then extend our analysis to the asymptotic effect of the perturbation on phase over many cycles (the phase response curve).

4.1. Initial effects of a small perturbation.

Assume that a trajectory begins on the stable limit cycle at position $x_0 = (1, u^\dagger)$ at time $t = 0$ and receives a small perturbation of size r

in the direction of a unit vector $\eta = (\eta_s, \eta_u)$ at time t'. We will consider only perturbations that occur before the trajectory leaves the square (i.e., $0 \le t' < T_1(u^\dagger) = T_1^\dagger$); earlier or later perturbations can be reduced to this case by an appropriate time shift and discrete rotation. We will also require that the perturbation not push the trajectory out of the basin of attraction of the limit cycle. The iPRC that we calculate below is obtained in the limit of small perturbations; for finite $a > 0$, the basin of attraction has finite width, and trajectories that escape the limit cycle's attracting set are not assigned an asymptotic phase.

It is straightforward to calculate the effects of the perturbation on the time and position at which the trajectory leaves the square. We first consider the typical case where the perturbation does not push the trajectory across the border of the square.

Lemma 6. *Consider a trajectory initially on the stable limit cycle γ of the iris system such that $\gamma(0) = (1, u^\dagger)$, and a perturbation Δx of size $||\Delta x|| = r$ in the direction of unit vector $\eta = (\eta_s, \eta_u) = \Delta x/r$ at time $0 < t' < T_1^\dagger$. Assume that the perturbation does not push the trajectory out of the basin of attraction or into another square. Then the perturbation will result in a change in the position of entry to the next square,*

$$\Delta u_1' = \big(\eta_s (u^\dagger e^{t'})^\lambda + \eta_u \lambda (u^\dagger)^{\lambda-1} e^{-t'}\big) r + o(r), \tag{4.1}$$

and a change in transit time of the square,

$$\Delta T_1' = -(\eta_u e^{-t'}/u^\dagger) r + o(r), \tag{4.2}$$

as $r \to 0$.

Proof. Immediately before the perturbation occurs, the trajectory will be at the point

$$\lim_{t \to t'-} x(t) = (e^{-\lambda t'}, u^\dagger e^{t'}).$$

The perturbation shifts the position to

$$\lim_{t \to t'+} x(t) = (e^{-\lambda t'} + r\eta_s, u^\dagger e^{t'} + r\eta_u).$$

The trajectory will exit the square once x_u grows to 1 at time

$$T_1' = t' + \big(-\log(u^\dagger e^{t'} + r\eta_u)\big)$$

and enter the next square along the $s = 1$ edge at position

$$u_1' = a + (e^{-\lambda t'} + r\eta_s) e^{-\lambda (T_1' - t')} = a + (e^{-\lambda t'} + r\eta_s)(u^\dagger e^{t'} + r\eta_u)^\lambda.$$

For $r \ll 1$, we may write

$$\begin{aligned} T_1' &= t' - \log(u^\dagger e^{t'}) - (\eta_u e^{-t'}/u^\dagger) r + o(r), \\ u_1' &= a + (u^\dagger)^\lambda + \big(\eta_s (u^\dagger e^{t'})^\lambda + \eta_u \lambda (u^\dagger)^{\lambda-1} e^{-t'}\big) r + o(r) \end{aligned}$$

as $r \to 0$. Noting that $t' - \log(u^\dagger e^{t'}) = -\log(u_i) = T_1^\dagger$ and $a + (u^\dagger)^\lambda = u^\dagger$, these expressions may be viewed as the exit time and position for the limit cycle with a linear correction and additional higher order terms in r. That is,

$$T_1' = T_1^\dagger - (\eta_u e^{-t'}/u^\dagger)r + o(r),$$
$$u_1' = u^\dagger + \left(\eta_s (u^\dagger e^{t'})^\lambda + \eta_u \lambda (u^\dagger)^{\lambda-1} e^{-t'}\right) r + o(r).$$

Subtracting $T_1^\dagger$ and $u^\dagger$ respectively then gives our result. ∎

Perturbations that push the trajectory across the boundary between two squares can be handled without much additional difficulty. For example, we can treat a perturbation that crosses into the next square as an advancement of the trajectory to the point that it enters the next square followed by a perturbation to the new location in the new square. Perturbations to the previous square can be handled in a similar fashion, as can perturbations to the diagonal square. However, for any finite $a > 0$ and any perturbation time other than $t' = 0$ or $t' = T_1^\dagger$, the perturbed point will remain in the same square as the unperturbed point for sufficiently small $r > 0$. Therefore the additional cases do not alter the calculation of the phase response curve except possibly at a finite set of points, and they will be omitted.

4.2. Subsequent effects of a perturbation. In the absence of perturbation, the limit cycle passing through $\gamma(0) = (1, u^\dagger)$ will exhibit a (constant) sequence of edge crossing locations $u_{i,n} = u^\dagger, n = \{0, 1, 2, \ldots\}$, at a sequence of crossing times $T_n^\dagger = nT_1^\dagger$ at constant intervals $\Delta T_n^\dagger \equiv T_1^\dagger$. A single perturbation $\Delta x = r(\eta_s, \eta_u)$ at time t' will lead to a new sequence of edge crossings $\{u_{i,n}'\}$ and crossing times $\{T_n'\}$. Following the perturbation, the time spent between the nth and $n+1$th crossings is offset from the unperturbed dwell time: $T_{n+1}' - T_n' = T_1^\dagger + \Delta T_{n+1}'$. Next we calculate the change in entry position for subsequent edge crossings ($\Delta u_n' = u_{i,n}' - u^\dagger$) and the dwell time offsets for subsequent squares ($\Delta T_{n+1}'$).

Lemma 7. *Under the conditions of Lemma 6, the entry position after the nth crossing ($n \geq 1$) will be offset by*

$$\Delta u_n' = \left(\lambda (u^\dagger)^{\lambda-1}\right)^{n-1} \left(\eta_s (u^\dagger e^{t'})^\lambda + \eta_u \lambda (u^\dagger)^{\lambda-1} e^{-t'}\right) r + o(r), \tag{4.3}$$

and the time spent in that square will be offset by

$$\Delta T_{n+1}' = -(u^\dagger)^{-1} \left(\lambda (u^\dagger)^{\lambda-1}\right)^{n-1} \left(\eta_s (u^\dagger e^{t'})^\lambda + \eta_u \lambda (u^\dagger)^{\lambda-1} e^{-t'}\right) r + o(r) \tag{4.4}$$

as $r \to 0$.

Proof. A perturbed trajectory will enter the nth edge with an offset $\Delta u_n'$. This situation is equivalent to a trajectory entering along the limit cycle that experiences a perturbation in the u direction ($\eta = (0, 1)$) of magnitude $r = \Delta u_n'$ immediately upon entering the square. We can thus use (4.1) with $t' = 0$ to find the entry position along the next ($n + 1$th) edge:

$$\Delta u_{n+1}' = \lambda (u^\dagger)^{\lambda-1} \Delta u_n' + o(\Delta u_n').$$

Therefore to leading order the sequence of offsets follows a geometric series, with closed form

$$\begin{aligned}\Delta u'_n &= \left(\lambda(u^\dagger)^{\lambda-1}\right)^{n-1}\Delta u'_1 + o(\Delta u'_1)\\ &= \left(\lambda(u^\dagger)^{\lambda-1}\right)^{n-1}\left(\eta_s(u^\dagger e^{t'})^\lambda + \eta_u\lambda(u^\dagger)^{\lambda-1}e^{-t'}\right)r + o(r)\end{aligned}$$

as $r \to 0$. Substitution into (4.2) provides the deviation in the time of passage through each square, compared with that for the limit cycle trajectory. Again setting $\eta = (0, 1)$, $r = \Delta u'_n$, and $t' = 0$ gives

$$\begin{aligned}\Delta T'_{n+1} &= -(u^\dagger)^{-1}\Delta u'_n + o(u'_n)\\ &= -(u^\dagger)^{-1}\left(\lambda(u^\dagger)^{\lambda-1}\right)^{n-1}\left(\eta_s(u^\dagger e^{t'})^\lambda + \eta_u\lambda(u^\dagger)^{\lambda-1}e^{-t'}\right)r + o(r). \qquad \blacksquare\end{aligned}$$

We now examine the asymptotic effect of the perturbation at long times. Because $u^\dagger$ is less than one, both Δu and Δt will approach zero for large n. This is equivalent to saying that the orbit will asymptotically return the stable limit cycle, as expected. It may, however, return with a different phase than the unperturbed trajectory.

Lemma 8. *Under the conditions of Lemma 6, the cumulative change in crossing times after n crossings is*

$$\Delta C'_n = -\frac{\eta_s(u^\dagger e^{t'})^\lambda\left(1-\left(\lambda(u^\dagger)^{\lambda-1}\right)^{n-1}\right) + \eta_u e^{-t'}\left(1-\left(\lambda(u^\dagger)^{\lambda-1}\right)^n\right)}{u^\dagger - \lambda(u^\dagger)^\lambda}r + o(r), \tag{4.5}$$

which converges to

$$\Delta C'_\infty = -\frac{\eta_s(u^\dagger e^{t'})^\lambda + \eta_u e^{-t'}}{u^\dagger - \lambda(u^\dagger)^\lambda}r + o(r) \tag{4.6}$$

as $n \to \infty$.

Proof. The cumulative change in crossing times is the sum of the dwell time offsets in the previous squares:

$$\Delta C'_n = \sum_{k=1}^{n}\Delta T'_k = \Delta T'_1 + \sum_{k=2}^{n}\Delta T'_k.$$

Substituting into (4.2) and (4.4) yields the result

$$\begin{aligned}\Delta C'_n &= -\frac{\eta_u e^{-t'}}{u^\dagger}r + \sum_{k=2}^{n}\frac{-r}{u^\dagger}\left(\lambda(u^\dagger)^{\lambda-1}\right)^{k-2}\left(\eta_s(u^\dagger e^{t'})^\lambda + \eta_u\lambda(u^\dagger)^{\lambda-1}e^{-t'}\right) + o(r)\\ &= \frac{-1}{u^\dagger}\left(\eta_u e^{-t'} + \left(\eta_s(u^\dagger e^{t'})^\lambda + \eta_u\lambda(u^\dagger)^{\lambda-1}e^{-t'}\right)\sum_{k=0}^{n-2}\left(\lambda(u^\dagger)^{\lambda-1}\right)^k\right)r + o(r)\\ &= \frac{-1}{u^\dagger}\left(\eta_u e^{-t'} + \left(\eta_s(u^\dagger e^{t'})^\lambda + \eta_u\lambda(u^\dagger)^{\lambda-1}e^{-t'}\right)\frac{1-\left(\lambda(u^\dagger)^{\lambda-1}\right)^{n-1}}{1-\lambda(u^\dagger)^{\lambda-1}}\right)r + o(r)\\ &= -\frac{\eta_s(u^\dagger e^{t'})^\lambda\left(1-\left(\lambda(u^\dagger)^{\lambda-1}\right)^{n+1}\right) + \eta_u e^{-t'}\left(1-\left(\lambda(u^\dagger)^{\lambda-1}\right)^n\right)}{u^\dagger - \lambda(u^\dagger)^\lambda}r + o(r).\end{aligned}$$

Recalling that $0 < u^\dagger < 1$ and $\lambda > 1$, taking the limit as $n \to \infty$ gives

$$\Delta C'_\infty = -\frac{\eta_s (u^\dagger e^{t'})^\lambda + \eta_u e^{-t'}}{u^\dagger - \lambda (u^\dagger)^\lambda} r + o(r),$$

as required. ∎

The limit cycle enters each square at location $(1, u^\dagger)$ and exits at $((u^\dagger)^\lambda, 1)$, so it is natural to define the exit coordinate along the stable eigenvector axis as $s^\dagger = (u^\dagger)^\lambda$. Recalling that $u^\dagger = s^\dagger + a$, (4.6) may be simplified as

$$\Delta C'_\infty = -\frac{\eta_s (s^\dagger e^{\lambda t'}) + \eta_u e^{-t'}}{u^\dagger - \lambda s^\dagger} r + o(r) = -\frac{\eta \cdot \beta}{u^\dagger - \lambda s^\dagger} r + o(r). \tag{4.7}$$

The vector $\beta = (s^\dagger e^{\lambda t'}, e^{-t'})$ may be thought of as a solution to the same differential equation as a trajectory within the first square, $\xi = (s, u)$, but with time reversed and initial conditions set to the far end of the square. That is,

$$\frac{d\xi}{dt} = \begin{pmatrix} -\lambda & 0 \\ 0 & 1 \end{pmatrix}, \qquad \xi(0) = \begin{pmatrix} 1 \\ u^\dagger \end{pmatrix},$$
$$\frac{d\beta}{dt} = \begin{pmatrix} \lambda & 0 \\ 0 & -1 \end{pmatrix}, \qquad \beta(0) = \begin{pmatrix} s^\dagger \\ 1 \end{pmatrix}.$$

4.3. The iPRC. We now derive the iPRC. Initially, we restrict our attention to perturbations occurring within the first quarter cycle, i.e., within the first square. The phase response curve for perturbations occurring after k additional border crossings is obtained via a discrete rotation operation.

We define the phase of a point on the limit cycle as in (2.3), i.e., as the smallest amount of time required to reach that point from the point where the limit cycle enters the first square. Therefore the asymptotic shift in crossing times translates into an asymptotic shift in phase as

$$\Delta\varphi = -\frac{4}{T}\Delta C'_\infty = -\frac{\Delta C'_\infty}{\log(1/u^\dagger)},$$

recalling that $T = 4T_1^\dagger = 4\log(1/u^\dagger)$. Since $e^{-t} = (u^\dagger)^\varphi$ we may write β in the form

$$\beta(\varphi) = (\beta_s(\varphi), \beta_u(\varphi)) = \left((u^\dagger)^{\lambda(1-\varphi)}, (u^\dagger)^\varphi\right) = \left((s^\dagger)^{(1-\varphi)}, (u^\dagger)^\varphi\right), \tag{4.8}$$

simplifying the subsequent analysis. Thus the asymptotic change in phase for a perturbation at phase $\varphi \in [0, 1)$ is

$$\Delta\varphi = \frac{\eta \cdot \beta(\varphi)}{\log(1/u^\dagger)(u^\dagger - \lambda s^\dagger)} r + o(r).$$

The iPRC, obtained by taking the limit of $\Delta\varphi/r$ as $r \to 0$, is therefore

$$Z(\eta, \varphi, a) = \frac{\eta \cdot \beta(\varphi)}{\log(1/u^\dagger)(u^\dagger - \lambda s^\dagger)},$$

which is (2.5).

For a perturbation at phase $\varphi \geq 1$, let k be the number of boundary crossings preceding the perturbation, i.e., the positive integer satisfying $\varphi \in [k, k+1)$. Define a k-fold quarter rotation operation on the phase variable and the direction of the perturbation by

$$\varphi \to \varphi' = \varphi - k, \tag{4.9}$$

$$\eta \to \eta' = \mathcal{R}^k \eta, \tag{4.10}$$

where $\mathcal{R} = \left(\begin{smallmatrix} 0 & -1 \\ 1 & 0 \end{smallmatrix}\right)$. Then the infinitesimal phase response due to a perturbation in direction η at phase $\theta > 0$ is given by $Z(\eta', \varphi', a)$.

The dependence of the phase response curve on the phase is entirely contained in the term $\eta \cdot \beta$. Consider the components of the response to perturbation in the horizontal and vertical directions. When $\varphi \in [0, 1)$, the component β_s along the direction of the stable eigenvector corresponds to β_x, the component in the horizontal direction. Similarly the components along the unstable direction β_u and the vertical component β_y are identical. Moving clockwise around one full orbit, we observe that

$$\begin{array}{llllll} \text{when} & \varphi \in [0,1), & \beta_x = \beta_s & \text{and} & \beta_y = \beta_u; \\ \text{when} & \varphi \in [1,2), & \beta_x = \beta_u & \text{and} & \beta_y = -\beta_s; \\ \text{when} & \varphi \in [2,3), & \beta_x = -\beta_s & \text{and} & \beta_y = -\beta_u; \\ \text{and when} & \varphi \in [3,4), & \beta_x = -\beta_u & \text{and} & \beta_y = \beta_s. \end{array}$$

For each component the resulting phase response curve consists of two continuous segments separated by a jump proportional to $(u^\dagger + s^\dagger)$, with antisymmetry $\beta(\varphi + 2) = -\beta(\varphi)$. The horizontal response component, β_x, peaks at $\beta_x(1) = 1$ and is strictly positive for $\varphi \in [0, 2)$. Similarly, β_y peaks at $\beta_y(0) = 1$ and is strictly positive for $\varphi \in [0, 1) \cup [3, 4)$. Hence the extrema of both components occur at phase values corresponding to the boundaries between adjacent squares.

Remark 9. *This concludes the proof of Theorem 1, part 2.*

Figure 8 shows examples of the full iPRCs as a function of $\theta \in [0, 4)$ for $\lambda = 2$ and $a \in \{10^{-3}, 0.1, 0.2, 0.24\}$.

5. Asymptotic phase resetting behavior as $a \to 0$. We wish to study the asymptotic behavior of the phase resetting curve at the heteroclinic limit, that is, as the parameter $a \to 0$. This limit corresponds, at least by analogy, with the limit $\mu \to 0$ in the smooth vector field system of equations (1.2).

Lemma 10. *Under the conditions of Lemma 6, the limit-cycle entry value scales as* $u^\dagger = a + o(a)$ *as* $a \to 0$.

Proof. Recall that $u^\dagger$ is the smaller root of $\rho(u)$, so $u^\dagger = a + (u^\dagger)^\lambda$. Since $\lambda > 1$, clearly $u^\dagger = a + o(u^\dagger)$ as $u^\dagger \to 0$, and $u^\dagger > a$ whenever $u^\dagger > 0$. For sufficiently small $a > 0$ we have $u^\dagger$ as an implicitly defined function of a. It is straightforward to see that $du^\dagger/da = 1$ when $u^\dagger = 0$. We wish to show that $u^\dagger = a + o(a)$ as well, i.e., that $\lim_{a\to 0}(u^\dagger - a)/a = 0$. Since $u^\dagger = a + o(a)$, for any $\epsilon > 0$ we can find a $\delta > 0$ such that $1 - a/u^\dagger < \min[\epsilon/2, 1/2]$ whenever $0 < u^\dagger < \delta$. If $a < \delta$, then $(u^\dagger - a)/a = 1/(1 - (1 - a/u^\dagger)) - 1 = 1/(1 - x) - 1 = x/(1 - x)$, where $x = 1 - a/u^\dagger$. Since $x < \min[\epsilon/2, 1/2]$, we are guaranteed that $x/(1 - x) < \epsilon$, as required. ∎

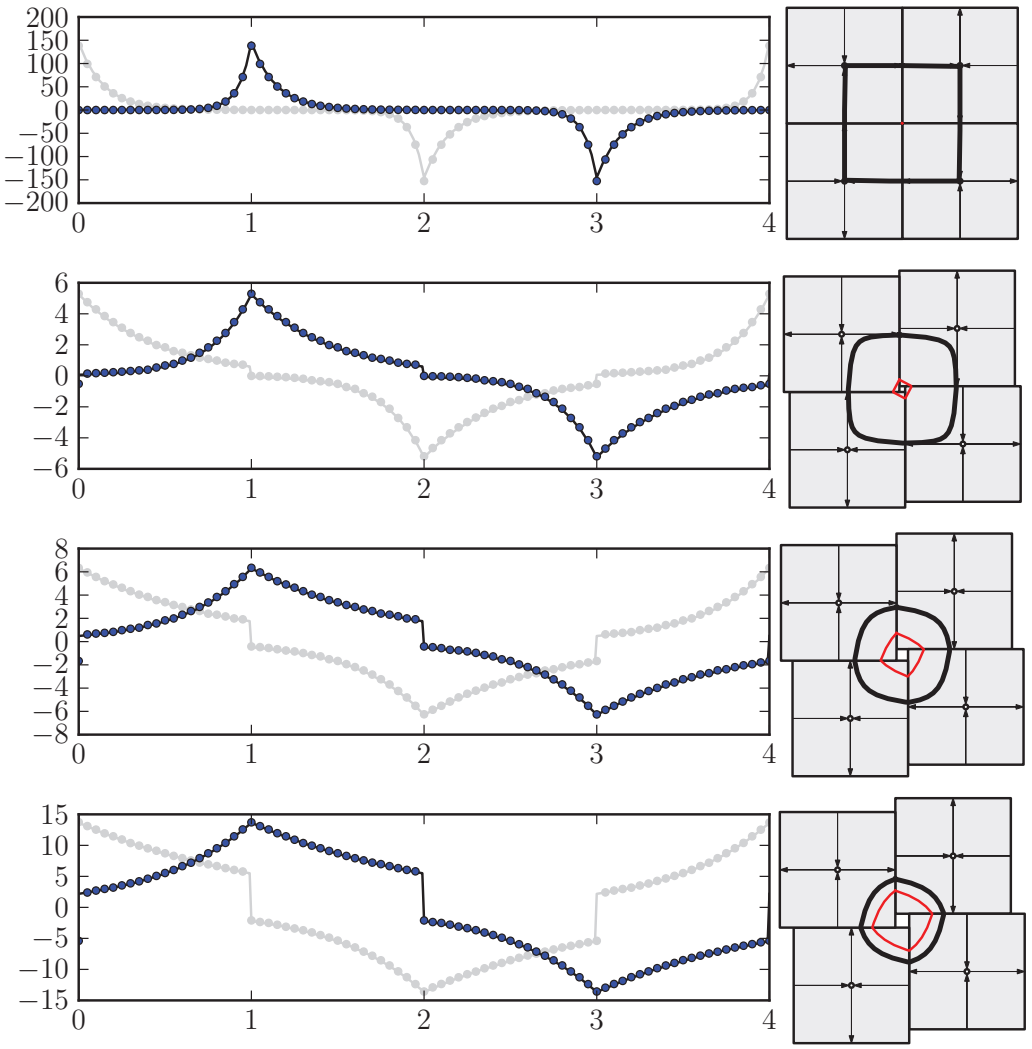

Figure 8. *The iPRCs for the iris system with various values of a. As a becomes small and the limit cycle approaches the heteroclinic orbit, the phase response curve becomes dominated by peaks at the edges between squares where flow changes from compressing trajectories outward to expanding them inward. As a grows and the flow along the limit cycle becomes more uniform, the iPRC becomes less sharply peaked. Line (dark blue): analytically obtained iPRC for a perturbation in the positive x direction. Points (dark blue): numerical iPRC, calculated using an instantaneous perturbation of 10^{-4} in the horizontal direction. From top to bottom, $a = 10^{-3}, 0.1, 0.2, 0.24$. The light gray curve represents the corresponding iPRC for perturbations in the vertical (positive y) direction. The discontinuities between the positive and negative portions of each curve are steps of height $(u^\dagger + s^\dagger)$ (see section 4.3 for further details).*

As a decreases, the peaks of the iPRC grow, while their width shrinks. The integral under each strictly positive region is

$$V = \int_0^2 \beta_x(\varphi)\, d\varphi = \frac{1 + \lambda - \lambda u^\dagger - (u^\dagger)^\lambda}{\lambda \log(1/u^\dagger)}, \tag{5.1}$$

which goes to zero as $u^\dagger \to 0$ or equivalently as $a \to 0$. Lemma 11 characterizes the behavior of the "normalized" iPRC $\alpha(\varphi) = \beta(\varphi)/V$ as $a \to 0$.

Lemma 11. *For the iris system the vector $\alpha(\varphi) = \beta(\varphi)/V$ has the following properties as $a \to 0$:*

1. *For $\varphi = 1$ or 3, $\alpha_x \to \pm\infty$, respectively. For $\varphi \notin \{1, 3\}$, $\alpha_x \to 0$.*
2. *For $\varphi = 0$ or 2, $\alpha_y \to \pm\infty$, respectively. For $\varphi \notin \{0, 2\}$, $\alpha_y \to 0$.*
3. *$\int_0^4 ||\alpha(\varphi)||\, d\varphi = 4$ (in the L_1 norm).*

Proof. As $a \to 0$ both $V \to 0$ and $u^\dagger \to 0$. At $\varphi = 1$, $\beta_x \equiv 1$ for all $a > 0$, so as $a \to 0$ the ratio $\beta_x(1)/V \to +\infty$. On the other hand, for fixed $\varphi \in [0, 2)\backslash\{1\}$, $\beta_x(\varphi)/V \to 0$ as $u^\dagger \to 0$. The behavior of α_x or α_y within the other intervals follows from the symmetry relations discussed in the preceding paragraph. Thus 1 and 2 are established. For 3, note that by construction each interval of length two centered on a peak of one component makes a unit contribution to the integral. That is,

$$1 = \int_{[0,2)} \alpha_x(\varphi)\, d\varphi = -\int_{[2,4)} \alpha_x(\varphi)\, d\varphi = -\int_{[1,3)} \alpha_y(\varphi)\, d\varphi = \int_{[3,4)\cup[0,1)} \alpha_y(\varphi)\, d\varphi.$$

The integral of the L_1 norm $||\alpha(\phi)||$ is the sum of these terms. ∎

Remark 12. *Lemma 11 and the symmetry of α together imply that each component of α converges weakly to a sum of delta function distributions on the circle:*

$$\alpha_x(\varphi) \to \delta(\varphi - 1) - \delta(\varphi - 3), \tag{5.2}$$

$$\alpha_y(\varphi) \to \delta(\varphi) - \delta(\varphi - 2) \tag{5.3}$$

as $a \to 0$.

Rewriting the full phase response curve in terms of α gives

$$Z(\eta, \varphi, a) = \frac{\eta \cdot \alpha(\varphi)\, V}{\log(1/u^\dagger)(u^\dagger - \lambda s^\dagger)} = (\eta \cdot \alpha(\varphi))\, M(u^\dagger), \tag{5.4}$$

where $M(u^\dagger) = \frac{1+\lambda-\lambda u^\dagger-(u^\dagger)^\lambda}{\lambda\left(\log(1/u^\dagger)\right)^2(u^\dagger-\lambda(u^\dagger)^\lambda)}$. The function M represents the magnitude of the phase response curve and diverges as $(u^\dagger \log^2(u^\dagger))^{-1}$ as $u^\dagger \to 0$.

The asymptotic phase response to an arbitrary instantaneous perturbation in direction η is a sum of the responses to the perturbation component along the stable eigenvector direction, η_s, and along the unstable eigenvector direction, η_u, within whichever square the perturbation occurs. The asymptotic behavior of the phase response in the heteroclinic limit for each component is distinct. We rewrite the phase response curve to emphasize these contributions thus (restricted, for convenience, to the lower left square, or $\varphi \in [0, 1)$):

$$Z(\eta, \varphi, a) = \frac{\eta_s\left((s^\dagger)^{(1-\varphi)}\right) + \eta_u\left((u^\dagger)^\varphi\right)}{\log(1/u^\dagger)(u^\dagger - \lambda s^\dagger)}. \tag{5.5}$$

First consider the response to perturbation along the unstable direction. Recall that, for any $p > 0$, $u^p \log u \to 0$ as $u \to 0^+$. It follows after a brief calculation that for any $\varphi \in [0, 1)$

$$\lim_{u\to 0^+} \left| \frac{u^\varphi}{\log(1/u)(u - \lambda u^\lambda)} \right| = +\infty.$$

This result means that, regardless of the phase of the perturbation, the sensitivity of the asymptotic phase to small displacements parallel to the unstable eigenvector diverges as the system approaches the heteroclinic bifurcation. The result is intuitively appealing because when the system is close to the heteroclinic bifurcation the long period leads to a larger "compounding" effect, enhancing the cumulative result of a small perturbation within a given square. However, as is often the case when dealing with nested limits, intuition can be misleading. In contrast to the preceding situation, consider the response to perturbation along the stable direction. The behavior of the limit now depends on the parameter λ:

$$\lim_{u\to 0^+}\left|\frac{u^{\lambda(1-\varphi)}}{\log(1/u)(u-\lambda u^{\lambda})}\right| = \begin{cases} 0, & \varphi\in[0,1-1/\lambda], \\ +\infty, & \varphi\in(1-1/\lambda,1). \end{cases}$$

Thus, in the heteroclinic limit, small perturbations parallel to the stable eigenvector become inconsequential if they occur at an early enough phase. At a particular phase,

$$\varphi_* = 1-\frac{1}{\lambda}, \tag{5.6}$$

the response becomes highly sensitive to arbitrarily small perturbation.

Remark 13. *This concludes the proof of Theorem 1, part 3.*

For comparison we can obtain from (3.4) the fractional phases at which the trajectory is closest to the saddle point (in the first square) or moving at the slowest speed:

$$\varphi_{\text{closest}} = \frac{1-\log\lambda/(2\log u^{\dagger})}{\lambda+1}, \qquad \varphi_{\text{slowest}} = \frac{1-3\log\lambda/(2\log u^{\dagger})}{\lambda+1}.$$

As $u^{\dagger}\to 0$ both phases converge to $\varphi_0 = 1/(\lambda+1)$, which is distinct from the phase at which the phase response curve's asymptotic sensitivity to perturbations in the stable direction changes. Curiously, the asymptotic value φ_0 of the phases of the slowest and closest point along the trajectory coincides with φ_*, the critical phase for sensitivity, precisely when λ is equal to the golden ratio, $(1+\sqrt{5})/2\approx 1.618\ldots$, because under those conditions $1-1/\lambda = 1/(\lambda+1)$.

6. Isochrons. Provided $a>0$ in the iris system, we may define isochrons as the level sets of the asymptotic phase function $\theta(x)$ for any point x in the basin of attraction of the limit cycle. As described in [12, 32, 35] and elsewhere, the points on a given isochron will converge over time to a single point on the limit cycle with a particular phase. Thus, in a sense, they represent points with the same asymptotic "time." As discussed above, given a limit cycle $\{\gamma(t)\}_{t=0}^{T_a}$, the asymptotic phase of a point x_0 is defined as the unique value in $\theta\in[0,\theta_{\max})$ such that the limit

$$\lim_{t\to\infty}|x(t)-\gamma(t+\theta(x_0))| = 0, \tag{6.1}$$

where $x(0)=x_0$ is the initial condition for the trajectory. The usual approach for finding isochrons is based on an adjoint equation method; cf. [12, Appendix A] and [26, Chapter 11]. From the chain rule, the phase field must satisfy

$$\frac{d}{dt}\theta(x(t)) = \left[\left(\vec{\nabla}\theta\right)(x(t))\right]\cdot\frac{dx}{dt} = \frac{\theta_{\max}}{T(a)}, \tag{6.2}$$

where $T(a)$ is the period of the limit cycle for a given value of $a > 0$. Let $(0 \le s \le 1, 0 \le u \le 1)$ be local coordinates relative to any saddle of the iris system, i.e., such that the flow satisfies $\dot{s} = -\lambda s$, $\dot{u} = u$. Writing θ_v for $\partial\theta/\partial v$, equation (6.2) reads

$$-\lambda s\theta_s + u\theta_u = \theta_{\max}/T(a). \tag{6.3}$$

By virtue of the fourfold rotational symmetry of the iris system, the following boundary conditions are required in addition to the PDE (6.2): for $0 < s < 1 - a$,

$$\theta(s, 1) = \theta(1, s + a) + 1. \tag{6.4}$$

The boundary condition renders the PDE nonlinear, and a simple closed form solution is not available. Solving the PDE numerically, however, is equivalent to finding the isochrons via direct simulation of trajectories for a suitable grid of initial conditions. We used a 400×400 square mesh of initial conditions within each square, tracking solutions until they either left the system of large squares (initial conditions on the interior of the unstable limit cycle) or converged with a suitable tolerance to a small neighborhood of the limit cycle, at which point the asymptotic phase could be assigned. Figure 9 shows an example of the isochrons generated with this technique.

7. Smooth system. In order to compare the family of iPRCs obtained for the iris system with that of a family of continuous vector fields experiencing a similar heteroclinic bifurcation with fourfold symmetry, we numerically evaluated the phase response for small instantaneous perturbations in the horizontal and vertical directions for limit cycles given by system (1.1) for positive values of the twist parameter μ. Figure 10 shows good qualitative agreement with the concentration of phase response sensitivity at points along the trajectory near integer values of the phase φ; cf. Figure 8.

8. Discussion. The iris system introduced here is one of only a handful of nonlinear dynamical systems for which an explicit form for the limit cycle or the phase response curve is known. For this system we show analytically that the sensitivity of the response to small instantaneous perturbations depends (as one would expect) on the distance to the heteroclinic bifurcation, on the phase at which the perturbation occurs, and on the direction of the perturbation in the phase plane. In addition, we find the intuitively appealing result that, regardless of phase, as the static perturbation away from the heteroclinic vector field diminishes, the phase response as measured by the iPRC becomes hypersensitive to any small perturbation parallel to the unstable eigenvector direction, in that the iPRC diverges as the bifurcation parameter of the iris system $a \to 0$. Unexpectedly, however, we also find that for perturbations along the *stable* eigenvector direction, the response to some will diverge while the response to others will have no effect in the limit as $a \to 0$. The system appears ultrasensitive in this case to the phase at which the perturbation occurs, with perturbations sufficiently far in advance of the approach towards the saddle point effectively absorbed by the flow, in contrast to perturbations beyond a critical phase, $\varphi_* = 1 - 1/\lambda$, which diverge as $a \to 0$. From a biological point of view, this dual sensitivity to the timing and direction of the transient perturbation is significant if flows structured by fixed points are to be exploited in nature as control points for rhythmic behaviors. In neural systems, for instance, it is commonplace

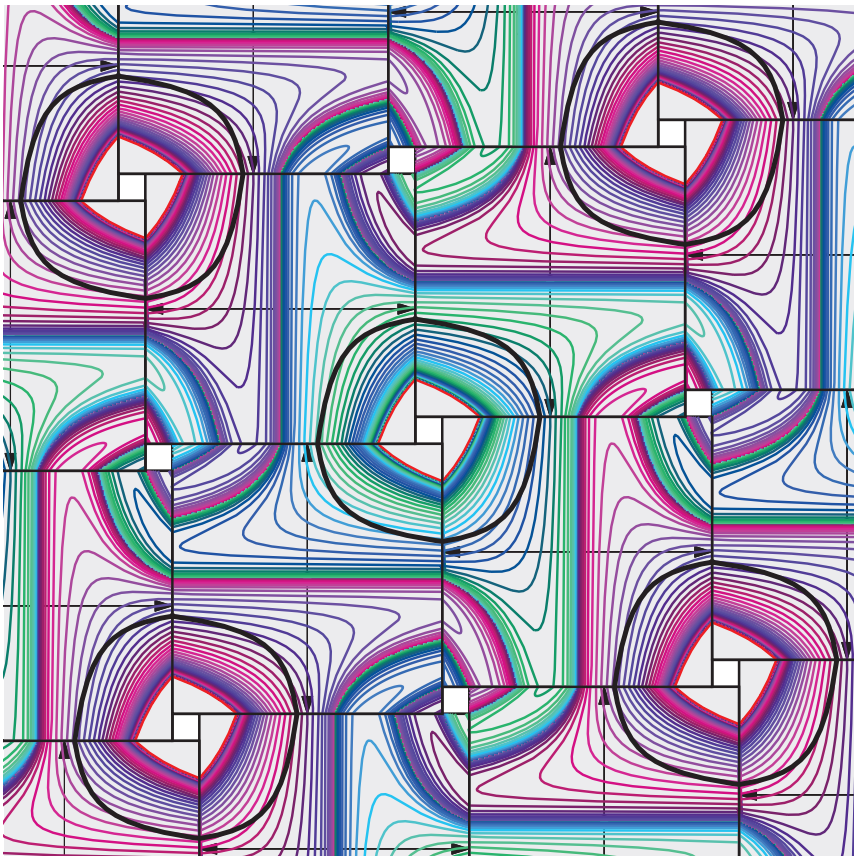

Figure 9. *Isochrons for the iris system obtained via numerical iteration of the map from initial conditions to a sequence of boundary crossing. The iris system on the torus has two distinct stable limit cycles for $a > 0$, illustrated here in two color schemes (green-blue and fuschia-violet). The tiling of the plane by periodic extension of the basic torus system is shown. Solid lines indicate the stable limit cycles; dashed lines indicate the unstable limit cycles. All limit cycles rotate clockwise. The flow inside the small squares is not defined, and points inside the unstable limit cycles are not part of the basin of attraction of the stable limit cycles. The stable manifolds of each saddle comprise the separatrices between the basins of attraction of distinct stable limit cycles. The system shown has $a = .2$ and $\lambda = 2$. Colors indicate the phase. Note the compression of the level curves near the boundaries between adjacent squares, which correspond to peaks in the phase response curve. Note also that the isochrons are* not *strictly parallel to the stable eigenvalue direction (cf. the discussion in section 8.2). Please see the corresponding movie* 82897_03.mpg [local/web 9.36MB]*; this animation illustrates the flow together with the isochron structure, by evolving points of equal phase forward together in time. After five seconds the animation changes to showing isochron structures for different values of the unstable/stable manifold offset parameter a, from $a = 0$ to $a = 0.247$ and back again.*

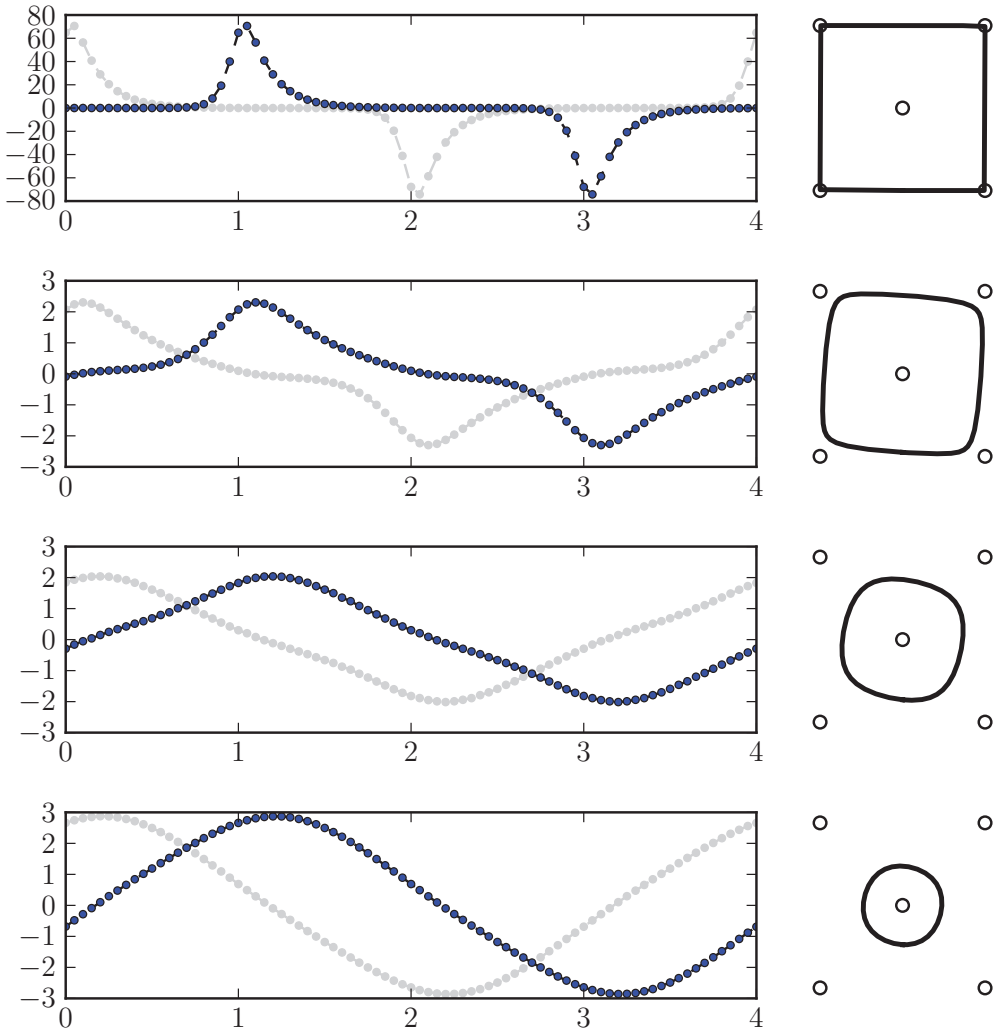

Figure 10. *The iPRCs for the smooth system with various values of μ. As μ becomes small and the limit cycle approaches the heteroclinic orbit, the phase response curve becomes dominated by peaks much like the iris system shown in Figure 8. As μ grows, the phase response curve becomes sinusoidal as the system approaches an Andronov–Hopf bifurcation. Points connected by dashed line (dark blue): numerical iPRC, calculated using an instantaneous perturbation of 10^{-4} in the horizontal direction. Dots (dark blue): iPRC for perturbations in the horizontal direction. Light gray: iPRC for perturbations in the vertical direction. From top to bottom, $\mu = 10^{-3}, 0.1, 0.3, 0.45$.*

to consider perturbations restricted to a single dimension in a multidimensional flow, namely perturbations along the dimension of membrane potential [12]. When a neuron's membrane potential lies in the linear regime, its dynamics are typically dissipative due to membrane conductances, tending to align the voltage direction with the stable direction for a subthreshold fixed point, at least for some portion of the flow. In general, if slowly adaptive modulatory processes within an organism's control circuitry can impose quasi-static perturbations of an

existing vector field to move trajectories closer to or farther away from a homo- or heteroclinic bifurcation point, the modulatory processes can filter which perturbations the system becomes sensitive to at different phases of the ongoing oscillation. Investigating these possibilities in specific systems such as the feeding CPG of the marine mollusk *Aplysia* will make it possible to test this prediction empirically.

8.1. Sensitivity and control. Our results suggest that, for systems in which a control parameter can change the approach of trajectories towards a hyperbolic saddle fixed point with a one dimensional unstable manifold, the sensitivity to specific kinds of perturbations could be actively managed by manipulating the critical phase φ_*. This is a novel kind of control for rhythmic behaviors; additional mechanisms for control include manipulating the period of a typical trajectory by controlling the time spent near a saddle point, and regulating the variable dwell time in different states for a limit cycle trajectory passing near multiple unstable fixed points.

Oscillations arising from codimension one bifurcations other than a saddle node-homoclinic have phase response curves near the bifurcation point that are smooth and sinusoidal. In contrast, many phase response curves observed in real systems show sharp transitions between small and large responses, even in systems generating highly regular behaviors such as swimming in the lamprey. Lamprey motor units participating in the CPG underlying smooth swimming show broad regions of near zero phase response combined with steep changes in sensitivity in other regions, going from zero to peak phase response in an interval corresponding to about 10% of the limit cycle duration (cf. Figure 6 of [72]). Preliminary data obtained from the marine mollusk *Aplysia californica* during feeding behavior show extended, variable dwell times in preferred regions of phase space separated by rapid transitions from region to region [57], suggesting the possibility that this CPG's dynamics may resemble those of a limit cycle making close encounters with a series of unstable fixed points.

The iPRC is equal to the gradient of the asymptotic phase function evaluated at the limit cycle. For the iris system, the level curves appear to pinch together at the boundaries where they abruptly change direction, and this pinching means the density of the level curves is highest at the square boundaries. One might naively expect that the phase response should be most sensitive to perturbations immediately adjacent to the saddle points; instead the peak sensitivity occurs at boundaries between regions dominated by one or another saddle. This effect is qualitatively present both in the PWL iris system and in the smooth system considered here. Within the PWL regions of the iris system the flow is homogeneous; it is the boundaries that make the system nonlinear, and it should not be surprising that that is where the greatest sensitivity occurs. In addition, the boundaries between PWL regions are the points at which the stable and unstable manifolds of adjacent saddles make their closest approach. In the sine system, it appears that near the saddles the flow is governed by the local linear approximation, while in the region between saddles the flow is "more nonlinear," coinciding with greater sensitivity to perturbation.

8.2. Comparison to the phase response curve near a homoclinic bifurcation. While the structure and asymptotic behavior of the phase response curve described in Theorem 1 were derived specifically for the iris system, we expect the qualitative picture to hold for generic one parameter families of limit cycles verging on a heteroclinic or a homoclinic bifurcation of

Table 1

Phase response curves for the standard homoclinic system (as in [12]), the quadratic integrate-and-fire (QIF) neuron, and the iris system, compared. For clarity, we write u, $0 < u < 1$, for $u^\dagger = \epsilon/\Delta$, and the phase $0 \le \varphi \le 1$ for both the iris and the standard homoclinic systems. Here $s = u^\lambda$; in the $\lambda \to \infty$ limit $s \to 0$, and the systems coincide (up to a scaling factor ν_x/Δ related to the choice of perturbation direction). The iPRC for perturbations parallel to the unstable (resp., stable) eigenvector direction is given by Z_u (resp., Z_s). The perturbation in the "stable" direction is not defined for the QIF model. See text for interpretation.

System	$Z_u(\varphi)$	$Z_s(\varphi)$
Saddle homoclinic [12]	$\dfrac{(\nu_x/\Delta)u^\varphi}{u\log(1/u)}$	0
Iris heteroclinic	$\dfrac{u^\varphi}{(u-\lambda s)\log(1/u)}$	$\dfrac{s^{(1-\varphi)}}{(u-\lambda s)\log(1/u)}$
QIF "saddle" homoclinic [35]	$\dfrac{((\mu+2)/\mu)^{1-\varphi}+((\mu+2)/\mu)^{\varphi-1}-2}{2\ln((\mu+2)/\mu)}$	-

C^1 vector fields as well. Treating the general case lies beyond the scope of this paper (but see section 8.5). However, it will be useful to compare our results with the analysis of phase resetting near a homoclinic bifurcation given in [12, section 3.1.3]. In section 8.3 we investigate the iPRC for the Morris–Lecar system near its homoclinic bifurcation. In the present section, we consider two analytic approximations of the iPRC for a "generic" near homoclinic orbit appearing in the literature [12, 35].

In [12] the authors consider a vector field on $\mathbb{R}^n$ with a hyperbolic saddle fixed point at the origin with a single unstable eigenvalue λ_u and stable eigenvalues $\lambda_{s,j}$ with $\lambda_u < \lambda_s = \min_j |\lambda_{s,j}|$. For positive values of a bifurcation parameter μ, the system is assumed to have a limit cycle that spends the overwhelming majority of its time in a box $B = [0, \Delta]^n$. Trajectories exit the box when the coordinate along the unstable eigendirection $x = \Delta$ and are instantaneously reinjected with $x = \epsilon$. When $n = 2$ the geometry is similar to that of the iris system (compare Figure 3 of [12] with our Figure 3(b)). The main difference is that in the homoclinic system, the value of the injection point along the unstable limit coordinate is assumed to be independent of the egress point, whereas in the iris system its dependence is specified by the map $h = f_e \circ f_l$ (Figure 6). Equivalently, it is as if the derivative of the function h were zero at the fixed point $u^\dagger$ rather than having finite slope. This situation would occur for the homoclinic system if the compression of the flow taking trajectories from the egress boundary to the ingress boundary were sufficiently great. However, in analyzing the homoclinic system, one must also assume that the time spent along the portion of the limit cycle outside the box B is vanishingly small. Reconciling these two limiting processes for the general homoclinic case remains an interesting problem.

For purposes of comparison, note that ϵ/Δ in [12] corresponds to $u^\dagger$ for the iris system, and the phase $\theta \in [0, 2\pi)$ in [12] corresponds to $2\pi\varphi$ in the iris system. Table 1 compares the iPRCs for the two systems. In [12] the perturbation is assumed to be in a particular direction, corresponding to a voltage deflection in a neural model; the factor ν_x arises in the change of coordinates from the direction of voltage perturbations relative to the unstable eigenvector direction. The flow is assumed to be infinitely compressive during the time between egress and reinjection, and consequently it is assumed that only components of the perturbation

along the unstable eigendirection contribute to the iPRC. This assumption holds for the iris system in the limit as the stable-to-unstable eigenvalue ratio $-\lambda_s/\lambda_u = \lambda \to \infty$, but not for finite values of λ. The $\lambda < \infty$ case includes additional corrections; see Table 1.

Finally, assuming that the phase response is independent of displacement along the stable eigenvector direction is equivalent to assuming that the isochrons run parallel to the stable eigenvector throughout the box B. For the iris system the slopes of the isochrons do approach zero as $\lambda \to \infty$, becoming more and more parallel to the stable eigenvector, but for $\lambda = \infty$ the asymptotic phase and the isochrons are no longer well defined. For finite values of λ the isochrons are well defined but are not parallel to the stable eigenvector. Compare the isochrons in the lower left quadrant of the iris system shown in Figure 9.

Another example of a system with a saddle homoclinic bifurcation is the quadratic integrate-and-fire (QIF) model neuron [35]. For example, consider the QIF system defined by the voltage equation

$$\dot{v} = v^2 - 1 \tag{8.1}$$

with reset to $v_0 = 1 + \mu$ whenever $v \to \infty$, which happens in finite time. For $\mu > 0$, this model produces a sequence of action potentials, or voltage resets, at times $t_k = t_0 + kT(\mu)$ with period

$$T(\mu) = \frac{1}{2} \ln\left(\frac{\mu + 2}{\mu}\right); \tag{8.2}$$

the period diverges logarithmically as $\mu \to 0^+$. The iPRC may be derived by taking the limit of small instantaneous perturbations of the voltage at times between resets. Defining the phase of the perturbation at time t^* as $\varphi = (t^* - t_0)/T(\mu) \mod 1$, one can show that the iPRC is

$$Z(\varphi, \mu) = \frac{\left(\frac{\mu+2}{\mu}\right)^{1-\varphi} + \left(\frac{\mu+2}{\mu}\right)^{\varphi-1} - 2}{2 \ln\left(\frac{\mu+2}{\mu}\right)}. \tag{8.3}$$

This quantity corresponds to the iPRC in the "unstable" direction for the planar homoclinic and heteroclinic iris systems. Because the QIF is a scalar model, there is no analogue of perturbations in the "stable" direction. If we evaluate the expression (8.3) at $\varphi \equiv 1$, corresponding to the "top" of the spike, we find for all $\mu > 0$ that $Z(0, \mu) = 0$. For all other phases $0 \le \varphi < 1$, the iPRC diverges to $+\infty$ as

$$Z(\varphi, \mu) \sim \frac{(2/\mu)^{1-\varphi}}{2 \ln(2/\mu)} \qquad (\text{as } \mu \to 0^+), \tag{8.4}$$

consistent with the calculation for the iris system and the standard planar homoclinic.

8.3. Qualitative comparison with a biological model: iPRCs for the Morris–Lecar system. Preparations are underway in our laboratory to test the sensitivity of rhythmic feeding behavior in the marine mollusk *Aplysia californica*, in both intact animals and in a semi-intact

suspended buccal mass preparation, to perturbations in the form of variable mechanical loading of the buccal mass during feeding. By using a servomotor to apply controlled forces to seaweed strands while the sea slug is ingesting them, it is possible to examine changes in the timing of the feeding rhythm in response to variable operating conditions. While the suspended buccal mass preparation includes the mouthparts and the ganglion comprising the feeding CPG, much of the proprioceptive feedback from the periphery to the central circuit is removed. Preliminary data show that the CPG of the reduced preparation produces qualitatively similar rhythms, but with longer dwell times at a sequence of quasi equilibria [57], suggesting the hypothesis that the underlying CPG lies closer to a homoclinic or heteroclinic structure in the absence of peripheral feedback. How well can we expect the differential sensitivity of the simple model systems considered here to compare with phase response curves in real biological systems operating near heteroclinic, or, more generically, homoclinic orbits? As a first step towards answering this question, we studied the iPRCs for a family of limit cycles verging on a homoclinic orbit in the classical Morris–Lecar equations [42, 54]. These equations describe the evolution of the voltage v and potassium gate w, and include a fast calcium current with gating variable m as well:

$$\frac{dv}{dt} = \frac{1}{C}\left(I_{app} - g_{Ca} m_\infty(v)(v - v_{Ca}) - g_K w (v - v_K) - g_L (v - v_L)\right), \tag{8.5}$$

$$\frac{dw}{dt} = \frac{w_\infty(v) - w}{\tau(v)}. \tag{8.6}$$

The terms m_∞, w_∞, and τ satisfy (for convenience we define $\xi = (v - v_c)/v_d$)

$$m_\infty = \frac{1}{2}\left(1 + \tanh\left(\frac{v - v_a}{v_b}\right)\right), \tag{8.7}$$

$$w_\infty(v) = \frac{1 + \tanh \xi}{2}, \tag{8.8}$$

$$\tau(v) = \frac{1}{\phi \cosh(\xi/2)}. \tag{8.9}$$

We used standard parameters from [26], near the bifurcation of a stable limit cycle to a saddle homoclinic orbit,

$$v_K = -84, \quad v_L = -60, \quad v_{Ca} = 120, \tag{8.10}$$

$$g_K = 8, \quad g_L = 2, \quad C = 20, \tag{8.11}$$

$$v_a = -1.2, \quad v_b = 18, \tag{8.12}$$

$$v_c = 12, \quad v_d = 17.4, \quad \phi = 0.23, \quad g_{Ca} = 4, \tag{8.13}$$

and studied the iPRC numerically for various values of the applied current, I_{app}. Figure 11 shows the numerically computed limit cycle trajectory for the Morris–Lecar system for applied currents $I_{app} \in \{40, 36.2, 35.05, 35.009\}$. For a modest injected current ($I_{app} = 40$) the model produces spikes with a period of $T = 24.0$ time units, and the iPRC is smooth and small, with values ranging from -0.6 to 0.4 (Figure 12, bottom). As I_{app} decreases, the interval between spikes increases, with $T = 39.0$ for $I_{app} = 36.2$, $T = 75.25$ for $I_{app} = 35.05$, and $T = 110.25$ for

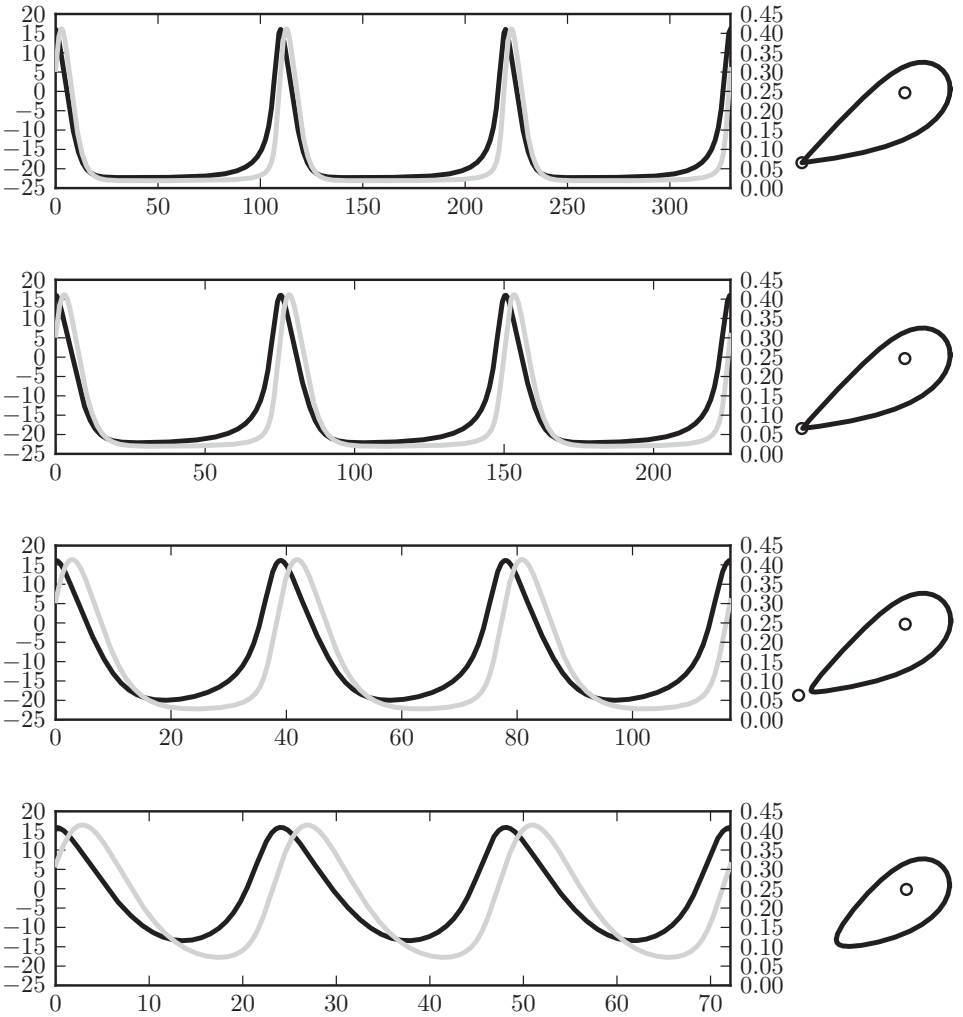

Figure 11. *Time plots of limit cycle trajectories of the Morris–Lecar system with various values of I_{app}. Left: voltage v and recovery variable w as functions of time (v: black trace, left scale; w: gray trace, right scale). Right: limit cycle trajectories in the (v, w) phase plane. Small circles indicate unstable fixed points (unstable nodes inside the limit cycles, and hyperbolic saddle fixed points outside). When $I_{app} \gtrsim I_* \approx 35.0067$ the time plots exhibit prolonged dwell times near the hyperbolic saddle (small circle near the bottom left of the limit cycle in the phase plane plot). As I_{app} increases, the limit cycle moves away from the saddle point, and the speed becomes more uniform. From top to bottom $I_{app} = 35.009, 35.05, 36.2, 40$. Compare Figures 2 and 5.*

$I_{app} = 35.009$. The limit cycle undergoes a saddle-homoclinic bifurcation at approximately $I_{app} = I_* \approx 35.0067$, at which point $T \to \infty$.

We obtained numerical estimates of the iPRC by applying small perturbations at different phases, with customized codes using open source tools (the scipy/numpy numerical libraries; see [36]). As the applied current is reduced towards this point, the iPRC grows in magnitude, reaching a range from -100 to $+75$ for $I_{app} = 35.009$. This dramatic increase in sensitivity is

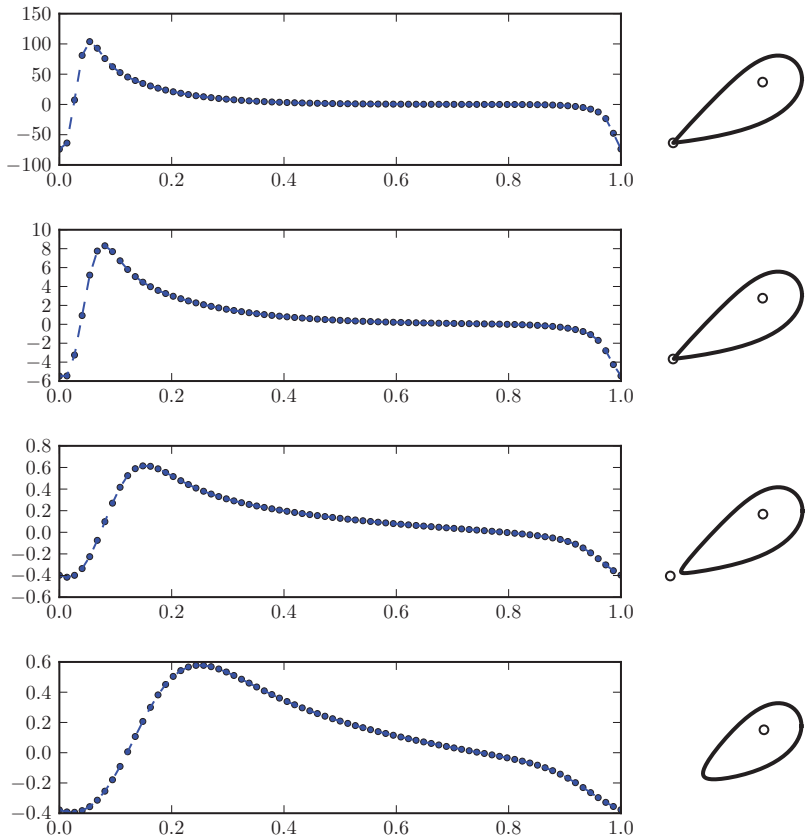

Figure 12. *The iPRCs for the Morris–Lecar system (equations (8.5)–(8.13)) with various values of the applied current I_{app}. Left: iPRC for voltage perturbations. The phase is normalized to the scale $0 \le \phi \le 1$, with $\phi = 0$ set to the maximum of the voltage trajectory. Right: trajectories in the (v,w) plane, with unstable fixed points denoted by open circles, as in Figure 11. Trajectories move counterclockwise about the interior fixed point. From bottom to top: $I_{app} = 40.0, 36.2, 35.05$, and 35.009. The homoclinic bifurcation occurs at approximately $I_{app} = 35.0067$ (equations integrated numerically with a Runge–Kutta scheme in XPP). As the applied current lessens, the limit cycle trajectory passes closer to the saddle point, and the iPRC grows larger. However, the most rapid growth in the iPRC appears to occur for phases away from the saddle (phases near $\phi = 0$), even as the system spends a growing fraction of time in small neighborhoods of the saddle. The saddle point is absent for $I_{app} = 40$.*

qualitatively consistent with our results, as well as with previous analyses of phase response curves near a homoclinic bifurcation (see [12] and [35, online section 10.4.3 and Figure 8.3]). However, we hasten to point out that the extrema of the iPRCs, plotted in Figure 12, appear to occur at phases φ lying *outside* a small neighborhood of the saddle point. For this system we define the zero phase as the phase corresponding to the peak of the voltage spike; hence the portion of the trajectory near the saddle point corresponds roughly to the broad flat region, e.g., $0.2 \lesssim \varphi \lesssim 0.9$ in the top panel of Figure 12. If we define a small neighborhood U enclosing the saddle point, it may be that the phase response diverges for phases φ such that $(v(t(\varphi)), w(t(\varphi))) \in U$, but our numerical results do not give strong evidence for or against this claim.

It is interesting to compare this situation with the iPRC for the QIF model (section 8.2). Referring to expression (8.3), we see that for any fixed value of $\mu > 0$ the greatest sensitivity to perturbation in the QIF model occurs immediately following the reset. Indeed, it is easy to show, for $0 \le \varphi < 1$ and $\mu > 0$, that $\partial Z(\varphi, \mu)/\partial\varphi < 0$. In section 10 of [35] (the online portion of the text), Figure 10.39 shows that the iPRC predicted by the QIF model diverges from that obtained numerically for a planar conductance-based model, with the greatest discrepancy between the two occurring immediately following the peak of the spike. Clearly, there is an opportunity for additional analysis of the asymptotic behavior of the sensitivity to perturbations in saddle-node homoclinic systems such as occur in the Morris–Lecar equations.

8.4. Stability of synchronous solutions for two iris systems with diffusive coupling. The iPRC is of interest for several reasons. One major application is analysis of synchronization behavior of coupled oscillators [25]. Dissipative or diffusive coupling—for instance, coupling of two oscillatory model neurons through a resistive linkage such as a gap junction—can lead to counterintuitive effects. Sherman and Rinzel [58] showed that while strong electrical coupling of bursting cells leads, as expected, to synchronous spiking within bursts, *weak* electrical coupling leads to *antiphase* synchrony of spikes within bursts. Moreover, this "microscopic" effect on spike timing leads to "macroscopic" effects such as extended burst duration, because appearance of the homoclinic trajectory in the slow variable, providing the mechanism for burst termination, was delayed by the shift in the trajectories caused by electrotonic coupling [21, 58]. The effect of weak coupling on convergence or divergence of nearby trajectories in pairs of cells typically varies around the limit cycle representing the oscillating uncoupled cell [37]; the coupling function (see (8.23) below) obtained by averaging around the limit cycle accounts for the net effect. A similar situation can arise when coupling two systems each of which follows a limit cycle that passes near a homoclinic orbit [37, Figure 2.8].

Consequently, it is interesting to investigate the stability of the synchronized solution for two iris systems coupled with diffusive coupling in one of the coordinates, for instance the horizontal coordinate, x. Consider an uncoupled iris system with a stable limit cycle described by a pair of ODEs

$$\dot{x} = F(x, y; a), \tag{8.14}$$

$$\dot{y} = G(x, y; a), \tag{8.15}$$

where $a > 0$ is the bifurcation parameter (the gap between the unstable and stable manifolds, W^u and W^s for successive saddles). As derived above, the limit cycle corresponds to an ingress point u relative to any given square, and an egress point $s = u^\lambda$, where $\lambda > 1$ is the saddle value. The ingress point for the limit cycle satisfies

$$u^\lambda - u + a = 0. \tag{8.16}$$

For instance, when $\lambda = 2$ and $a = 0.01$ we have $u \approx 0.0102\ldots$ and $s \approx 1.0205 \times 10^{-4}$. The period of the limit cycle is $T = 4\ln(1/u)$, and we define the phase as $\phi(t) = 4t/T$, with zero phase chosen to be the point of ingress to the lower left square. Hence we have $\phi \in [0, 1)$ for the first (lower left) square, $\phi \in [1, 2)$ for the second square, $\phi \in [2, 3)$ for the third square,

and $\phi \in [3,4)$ for the last square. The iPRC for perturbations in the horizontal direction is given by

$$Z(\phi) = \begin{cases} Ks^{1-\phi}, & \phi \in [0,1), \\ Ku^{\phi-1}, & \phi \in [1,2), \\ -Ks^{3-\phi}, & \phi \in [2,3), \\ -Ku^{\phi-3}, & \phi \in [3,4), \end{cases} \tag{8.17}$$

where $K > 0$ is a constant that is common to all terms, namely $K = [\ln(1/u)(u - \lambda s)]^{-1} > 0$. A pair of iris systems with diffusive coupling is now described by four equations:

$$\dot{x}_1 = F(x_1, y_1; a) + k(x_2 - x_1), \tag{8.18}$$

$$\dot{x}_2 = F(x_2, y_2; a) + k(x_1 - x_2), \tag{8.19}$$

$$\dot{y}_1 = G(x_1, y_1; a), \tag{8.20}$$

$$\dot{y}_2 = G(x_2, y_2; a). \tag{8.21}$$

If $x = u(t)$, $y = v(t)$ is a stable limit cycle solution for an uncoupled iris system (for $a > 0$), we wish to know whether or not for $k > 0$ the synchronous solution $x_1 = x_2 = u(t)$, $y_1 = y_2 = v(t)$ is stable.

Following standard weak coupling arguments [26], we can represent the solutions to the coupled systems in terms of their phases as defined for the uncoupled system, $x(\phi)$ and $y(\phi)$. The two coupled systems with a (small) phase difference $\chi = \phi_2 - \phi_1$ evolve according to

$$\dot{\chi} = H(-\chi) - H(\chi) + o(\chi), \tag{8.22}$$

where the H-function is defined as

$$H(\chi) = \frac{k}{4} \int_{\phi=0}^{4} Z(\phi)(x(\phi + \chi) - x(\phi))\, d\phi. \tag{8.23}$$

The roots of the expression $H(-\chi) - H(\chi) = 0$ are fixed points for the evolution of χ, and $\chi = 0$ corresponds to the synchronous solution. The stability of the synchronous solution depends on the sign of $d/d\chi(H(-\chi) - H(\chi)) = -2H'(0)$ at $\chi = 0$. If this quantity is negative, we have stable synchrony. If it is positive, synchrony is unstable.

For the PWL iris system, we have explicit expressions for the trajectory $x(\phi)$, using $s = u^{\lambda}$:

$$x(\phi) = \begin{cases} \frac{u-s}{2} - (1 - s^{\phi}), & \phi \in [0,1), \\ \frac{s-u}{2} - (1 - u^{2-\phi}), & \phi \in [1,2), \\ \frac{s-u}{2} + (1 - s^{\phi-2}), & \phi \in [2,3), \\ \frac{u-s}{2} + (1 - u^{4-\phi}), & \phi \in [3,4). \end{cases} \tag{8.24}$$

Figure 13 shows the trajectory $x(\phi)$, iPRC (x-component) $Z_x(\phi)$, and derivative of the trajectory $dx/d\phi$, for $a = 0.02$.

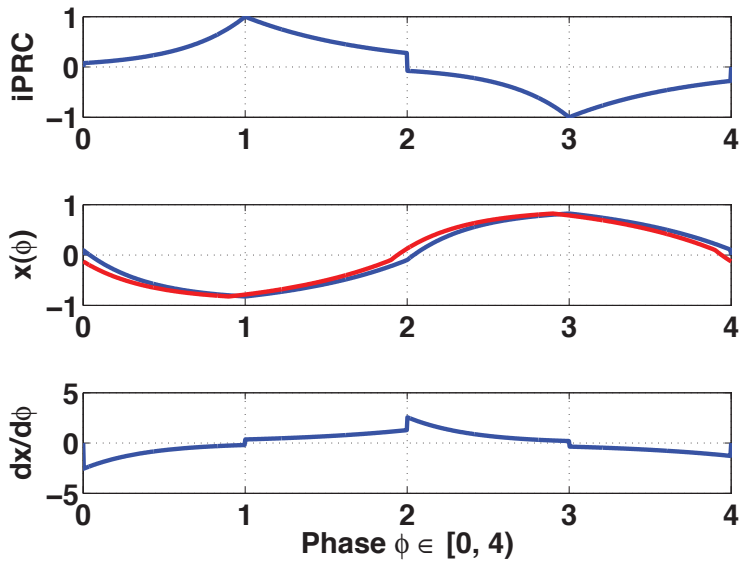

Figure 13. *The iPRC and trajectory for the iris system (x-component) with twist parameter $a = 0.02$. Top: the x-component of the iPRC, $Z_x(\phi)$ (neglecting a positive constant K). Middle: the x-component of the trajectory, $x(\phi)$ (blue), and the same trajectory lagged by $\Delta\phi = 0.1$ (red). Bottom: the derivative $dx/d\phi(\phi)$.*

It is straightforward to obtain the necessary derivative at $\chi = 0$, namely,

$$H'(0) = \left[\frac{k}{4}\int_{\phi=0}^{4} Z(\phi)\left(x'(\phi+\chi)\right)\right]\Big|_{\chi=0} = \frac{k}{4}\int_0^4 Z(\phi)\frac{dx}{d\phi}(\phi)\,d\phi. \tag{8.25}$$

The derivatives of the trajectory x with respect to the phase ϕ are

$$\frac{dx}{d\phi} = \begin{cases} s^{\phi}\ln s, & \phi\in[0,1),\\ -u^{2-\phi}\ln u, & \phi\in[1,2),\\ -s^{\phi-2}\ln s, & \phi\in[2,3),\\ u^{4-\phi}\ln u, & \phi\in[3,4). \end{cases} \tag{8.26}$$

Remarkably, the ϕ-dependence drops out of the integrands, giving the following (recalling that $K = [\ln(1/u)(u-\lambda s)]^{-1} > 0$ and $s = u^{\lambda}$):

$\phi\in I$	$Z(\phi)$	$\frac{dx}{d\phi}$	$Z(\phi)\frac{dx}{d\phi}$	$\int_I \left(Z(\phi)\frac{dx}{d\phi}(\phi)\right)\,d\phi$
$I=[0,1)$	$Ks^{1-\phi}$	$s^{\phi}\ln s$	$Ks\ln s$	$Ks\ln s$
$I=[1,2)$	$Ku^{\phi-1}$	$-u^{2-\phi}\ln u$	$-Ku\ln u$	$-Ku\ln u$
$I=[2,3)$	$-Ks^{3-\phi}$	$-s^{\phi-2}\ln s$	$Ks\ln s$	$Ks\ln s$
$I=[3,4)$	$-Ku^{\phi-3}$	$u^{4-\phi}\ln u$	$-Ku\ln u$	$-Ku\ln u$

Therefore,

$$H'(0) = \frac{k}{4}K\left(2s\ln s - 2u\ln u\right) = \frac{k}{2}\frac{\lambda s\ln u - u\ln u}{\ln(1/u)(u-\lambda s)} = \frac{k}{2}. \tag{8.27}$$

Thus for $k > 0$ this result indicates stabilization of the synchronous solution, for this system, under weak diffusive coupling along the x-direction. This result was confirmed by numerical simulations.

Remark 14. *While the calculation above holds at a finite distance from the heteroclinic bifurcation (i.e., setting the twist parameter $a > 0$), the results do not appear to carry over to the heteroclinic bifurcation point ($a = 0$). Indeed, for the piecewise linear iris system, in this case the unperturbed trajectories coincide with the stable/unstable manifolds of each saddle. Because of the system geometry, diffusive coupling in the x-coordinate alone will cause nearby trajectories to approach each other if they are separated in phase, but they will never leave the orbit connecting two adjacent saddles and hence remain "synchronized." On the other hand, if one trajectory is perturbed* off *the uncoupled orbit by a small amount towards the interior of the heteroclinic cycle, that trajectory will pass the next saddle point in finite time. If it only exerts a perturbation parallel to the horizontal direction, say, on the other trajectory, it will not help the other get around the corner. Therefore one trajectory will orbit near the heteroclinic path, while the other trajectory oscillates back and forth on the line connecting two horizontally displaced saddles. This situation will hold for any transverse initial perturbation (near the zero phase point, for example) no matter how small, and hence the diffusive coupling does not stabilize the "synchronous" solution in this case.*

This situation is dependent on the particular geometry of the iris system, and would not necessarily obtain in systems with different geometry. The coupling could, for instance, perturb trajectories along a different direction. For the Morris–Lecar system near the homoclinic bifurcation, one can apply a change of coordinates at the saddle point with respect to which the stable and unstable eigenvectors become orthogonal. In the new coordinates, "diffusive" coupling mediated by the voltage difference acts along a direction at some angle with respect to the stable and unstable eigenvectors, ξ_s and ξ_u. Whether diffusive coupling stabilizes or destabilizes the synchronous solution then depends on the detailed geometry of the trajectories near the homoclinic. If we consider diffusive-like coupling in an arbitrary direction for a pair of identical iris systems, when they are located at the heteroclinic point we have an evolution given by 2^4 sets of linear maps in subsets of $\mathbb{R}^4$. Intuitively, many complicated and interesting trajectories, both periodic and aperiodic, could occur.

8.5. Generalization to higher dimensional systems. Consider a smooth dynamical system dynamical system in $\mathbb{R}^n$, $\dot{x} = F(x, \mu)$. Suppose there are constants $\mu_- < 0 < \mu_+$ and an interval $I = \{\mu | \mu_- < \mu < \mu_+\}$ for which the following assumptions hold:

- For all $\mu \in I$, there is a hyperbolic saddle fixed point at the origin, $F(0, \mu) = 0$, with one dimensional unstable manifold W^u and $(n-1)$ dimensional stable manifold W^s.
- For $\mu > 0$ and $\mu \in I$, there is a smooth family of orbitally stable limit cycles colliding transversely with a saddle homoclinic loop at the origin, at $\mu = 0$.
- For all $\mu \geq 0$, $\mu \in I$, the single unstable eigenvalue $\lambda_u(\mu) > 0$ is smaller than $-\lambda_s(\mu)$, where λ_s is the stable eigenvalue with negative real part closest to zero.
- For all $\mu \in I$, there is an open neighborhood $U \subset \mathbb{R}^n$ of the origin within which the flow is "sufficiently close" (in some appropriate sense) to the linear flow given by $\dot{x} = DF(0, \mu) \cdot x$.

Suppose we define, for this system, "zero phase" to be the phase at which the limit cycle enters the (fixed, small) neighborhood U enclosing the origin. Under the hypotheses above,

it would not be unreasonable to anticipate the following:

- The iPRC, $Z_u(\phi;\mu)$, for perturbations parallel to the unstable eigenvector direction diverges as $\mu \to 0^+$ for all phases ϕ with corresponding trajectory location $x(\phi) \in U$.
- There will be a subspace S_1 of $\mathbb{R}^n$ tangent to $x = 0$, and a phase ϕ_1, such that the iPRC, $Z_1(\phi;\mu)$, for perturbations restricted to S_1 will converge to zero as $\mu \to 0^+$ for phases $\phi \in (0, \phi_1]$. For phases $\phi > \phi_1$ we would anticipate the existence of perturbations within S_1 that lead to divergent phase responses.
- There may be additional subspaces $S_{k+1} \subset S_k$ and phases $\phi_{k+1} > \phi_k$ with the property that the iPRC, $Z_k(\phi,\mu)$, for perturbations restricted to the subspace S_k will converge to zero for phases $\phi \in (0, \phi_k]$ as $\mu \to 0^+$. For phases $\phi > \phi_k$ we expect that perturbations within $S_k \backslash S_{k+1}$ will diverge as $\mu \to 0^+$.

If this intuition should be borne out, it would indicate the existence of a nested hierarchy of subspaces at the saddle point, corresponding to greater and greater ability to "absorb" perturbation applied in particular directions. The reasoning behind this conjecture is that near a saddle point the $(n-1)$ dimensional stable manifold will be converging towards $x = 0$ at different exponential rates along different eigendirections of the linearization $DF(0,\mu)$. Perturbations in directions corresponding to more rapidly decaying components, i.e., those with larger negative eigenvalues, will be damped more quickly, and therefore will be less destabilizing, than perturbations in other more unstable directions.

8.6. Phase resetting in the absence of an asymptotic phase. The ability to produce a wide variety of stable phase relationships (intermediate phase locked states; cf. [71]) is an important aspect of CPGs and may be important for their adaptive control. As an example, Szücs et al. [67] observed synchronization of pairs of CPGs in separate animals coupled artificially through a variety of configurations using extended dynamic clamp [47]. Simulated diffusive (electrical) coupling led to synchronization only for sufficiently large simulated conductances, while simulated contralateral inhibition from lateral pyloric (LP) to pyloric dilator (PD) pacemaker neurons was more effective at inducing 1:1 synchronized phase locking, as was mutual inhibition between the PD neurons. Mutually inhibitory reciprocal synaptic connections between bursting cells can be one mechanism for generating stable heteroclinic sequences [45]. Prolonged intervals separating switches between distinct phase-locked states was also studied in terms of a heteroclinic loop in a coupled oscillator system in [38].

Although many applications of phase response curve calculations focus on coupling, the iPRC is a helpful conceptual tool in other settings as well. For instance, Nadim et al. [43] showed that inhibitory feedback within a CPG served to reduce the variability in duration of a specific burst phase by flattening the iPRC, providing a mechanism for control and phase stabilization of a CPG.

Deterministic limit cycles are not the only way to represent (approximately) periodic biological rhythms. Alternatives include heteroclinic or homoclinic attractors perturbed by small amplitude noise [8, 64] as well as fixed points of spiral sink type subject to small noisy perturbations [10, 35]. A system comprising a deterministic flow with a stable spiral fixed point, when perturbed by small to modest amounts of noise, will show noisy oscillatory trajectories that can be difficult to distinguish from a small amplitude limit cycle [10]. For example, the small oscillations in membrane potential of a nerve cell brought near to firing

by a steady depolarizing current of modest size may be due either to "noisy spiral sink" dynamics or to "noisy small limit cycle" dynamics [61]. The classical definition of asymptotic phase breaks down for noisy systems, for spiral sinks, and for heteroclinic or homoclinic orbits. Nevertheless "phase resetting" is actively studied in such systems both experimentally [23, 24, 61, 62] and theoretically [33, 52, 51]. For the Bonhoeffer–van der Pol equations, for example, Rabinovitch and Rogachevskii showed how to define an analogue of the classical isochron, for points converging to a spiral sink along a distinguished trajectory (a "T-attractor") [52] (see also [33]). Generally speaking, noise effects can expose the structure of bifurcations in neural systems through stochastic resonance [28] or spike time bifurcations [68, 69], and it would be useful to have a broader theory of "phase response" going beyond the case of deterministic limit cycles.

Acknowledgments. The authors thank C. Turc and W. Guo for helpful discussion concerning solutions of the adjoint equation, and S. Coombes, G. B. Ermentrout, R. Galan, A. Horchler, D. Terman, and the reviewers of the previous version of the manuscript for helpful discussion or comments. P. J. T. thanks the Mathematical Biosciences Institute for their hospitality during the completion of this work.

REFERENCES

[1] V. Afraimovich, F. C. Ordaz, and J. Urias, *A class of cellular automata modeling winnerless competition*, Chaos, 12 (2002), pp. 279–288.
[2] V. Afraimovich, I. Tristan, R. Huerta, and M. I. Rabinovich, *Winnerless competition principle and prediction of the transient dynamics in a Lotka-Volterra model*, Chaos, 18 (2008), 043103.
[3] V. Afraimovich, T. Young, M. K. Muezzinoglu, and M. I. Rabinovich, *Nonlinear dynamics of emotion-cognition interaction: When emotion does not destroy cognition?*, Bull. Math. Biol., 73 (2011), pp. 266–284.
[4] V. S. Afraimovich, M. I. Rabinovich, and P. Varona, *Heteroclinic contours in neural ensembles and the winnerless competition principle*, Internat. J. Bifur. Chaos Appl. Sci. Engrg., 14 (2004), pp. 1195–1208.
[5] V. S. Afraimovich, V. P. Zhigulin, and M. I. Rabinovich, *On the origin of reproducible sequential activity in neural circuits*, Chaos, 14 (2004), pp. 1123–1129.
[6] A. A. Andronov and L. S. Pontryagin, *Systèmes grossiers*, Dokl. Akad. Nauk. SSSR, 14 (1937), pp. 247–251.
[7] D. Armbruster, E. Stone, and V. Kirk, *Noisy heteroclinic networks*, Chaos, 13 (2003), pp. 71–79.
[8] Y. Bakhtin, *Noisy heteroclinic networks*, Probab. Theory Related Fields, 150 (2011), pp. 1–42.
[9] R. D. Beer, H. J. Chiel, and J. C. Gallagher, *Evolution and analysis of model CPGs for walking: II. General principles and individual variability*, J. Comput. Neurosci., 7 (1999), pp. 119–147.
[10] R. P. Boland, T. Galla, and A. J. McKane, *How limit cycles and quasi-cycles are related in systems with intrinsic noise*, J. Statist. Mech., 2008 (2008), P09001.
[11] D. S. Boukal and V. Křivan, *Lyapunov functions for Lotka-Volterra predator-prey models with optimal foraging behavior*, J. Math. Biol., 39 (1999), pp. 493–517.
[12] E. Brown, J. Moehlis, and P. Holmes, *On the phase reduction and response dynamics of neural oscillator populations*, Neural. Comput., 16 (2004), pp. 673–715.
[13] J. T. Buchanan and A. H. Cohen, *Activities of identified interneurons, motoneurons, and muscle fibers during fictive swimming in the lamprey and effects of reticulospinal and dorsal cell stimulation*, J. Neurophysiol., 47 (1982), pp. 948–960.
[14] P. L. Buono and M. Golubitsky, *Models of central pattern generators for quadruped locomotion. I. Primary gaits*, J. Math. Biol., 42 (2001), pp. 291–326.
[15] H. J. Chiel, R. D. Beer, and J. C. Gallagher, *Evolution and analysis of model CPGs for walking: I. Dynamical modules*, J. Comput. Neurosci., 7 (1999), pp. 99–118.

[16] A. H. Cohen, G. B. Ermentrout, T. Kiemel, N. Kopell, K. A. Sigvardt, and T. L. Williams, *Modelling of intersegmental coordination in the lamprey central pattern generator for locomotion*, Trends Neurosci., 15 (1992), pp. 434–438.
[17] S. Coombes, *Neuronal networks with gap junctions: A study of piecewise linear planar neuron models*, SIAM J. Appl. Dyn. Syst., 7 (2008), pp. 1101–1129.
[18] S. Coombes and P. C. Bressloff, eds., *Bursting: The Genesis of Rhythm in the Nervous System*, World Scientific, River Edge, NJ, 2005.
[19] S. Coombes and A. H. Osbaldestin, *Period-adding bifurcations and chaos in a periodically stimulated excitable neural relaxation oscillator*, Phys. Rev. E (3), 62 (2000), pp. 4057–4066.
[20] E. De Schutter, J. D. Angstadt, and R. L. Calabrese, *A model of graded synaptic transmission for use in dynamic network simulations*, J. Neurophysiol., 69 (1993), pp. 1225–1235.
[21] G. De Vries, A. Sherman, and H. R. Zhu, *Diffusively coupled bursters: Effects of cell heterogeneity*, Bull. Math. Biol., 60 (1998), pp. 1167–1200.
[22] R. Edwards and L. Glass, *Combinatorial explosion in model gene networks*, Chaos, 10 (2000), pp. 691–704.
[23] B. Ermentrout and D. Saunders, *Phase resetting and coupling of noisy neural oscillators*, J. Comput. Neurosci., 20 (2006), pp. 179–190.
[24] G. B. Ermentrout, R. F. Galán, and N. N. Urban, *Reliability, synchrony and noise*, Trends Neurosci., 31 (2008), pp. 428–434.
[25] G. B. Ermentrout and N. Kopell, *Frequency plateaus in a chain of weakly coupled oscillators*, I., SIAM J. Math. Anal., 15 (1984), pp. 215–237.
[26] G. B. Ermentrout and D. H. Terman, *Foundations of Mathematical Neuroscience*, Springer, New York, 2010.
[27] A. F. Filippov, *Differential Equations with Discontinuous Righthand Sides*, Math. Appl. 18, Kluwer Academic Publishers, Dordrecht, The Netherlands, 1988.
[28] Y. Gai, B. Doiron, and J. Rinzel, *Slope-based stochastic resonance: How noise enables phasic neurons to encode slow signals*, PLoS Comput. Biol., 6 (2010), e1000825.
[29] L. Glass and J. S. Pasternack, *Prediction of limit cycles in mathematical models of biological oscillations*, Bull. Math. Biol., 40 (1978), pp. 27–44.
[30] L. Glass and J. S. Pasternack, *Stable oscillations in mathematical models of biological control systems*, J. Math. Biol., 6 (1978), pp. 207–223.
[31] M. Golubitsky, I. Stewart, P. L. Buono, and J. J. Collins, *Symmetry in locomotor central pattern generators and animal gaits*, Nature, 401 (1999), pp. 693–695.
[32] J. Guckenheimer and P. Holmes, *Nonlinear Oscillations, Dynamical Systems, and Bifurcations of Vector Fields*, 3rd ed., Appl. Math. Sci. 42, Springer-Verlag, Berlin, 1990.
[33] N. Ichinose, K. Aihara, and K. Judd, *Extending the concept of isochrons from oscillatory to excitable systems for modeling an excitable neuron*, Internat. J. Bifur. Chaos Appl. Sci. Engrg., 8 (1998), pp. 2375–2385.
[34] A. J. Ijspeert, *Central pattern generators for locomotion control in animals and robots: A review*, Neural. Netw., 21 (2008), pp. 642–653.
[35] E. M. Izhikevich, *Dynamical Systems in Neuroscience: The Geometry of Excitability and Bursting*, Computational Neuroscience, MIT Press, Cambridge, MA, 2007.
[36] E. Jones, T. Oliphant, and P. Peterson, *SciPy: Open source scientific tools for Python*, 2001; available online at http://www.scipy.org.
[37] N. Kopell and G. B. Ermentrout, *Mechanisms of phase-locking and frequency control in pairs of coupled neural oscillators*, in Handbook of Dynamical Systems, B. Fiedler, ed., North–Holland, Amsterdam, 2002, pp. 3–54.
[38] H. Kori and Y. Kuramoto, *Slow switching in globally coupled oscillators: Robustness and occurrence through delayed coupling*, Phys. Rev. E (3), 63 (2001), 046214.
[39] V. Křivan and I. Vrkoč, *A Lyapunov function for piecewise-independent differential equations: Stability of the ideal free distribution in two patch environments*, J. Math. Biol., 54 (2007), pp. 465–488.
[40] S. N. Markin, A. N. Klishko, N. A. Shevtsova, M. A. Lemay, B. I. Prilutsky, and I. A. Rybak, *Afferent control of locomotor CPG: Insights from a simple neuromechanical model*, Ann. N.Y. Acad. Sci., 1198 (2010), pp. 21–34.
[41] H. P. McKean, *Nagumo's equation*, Adv. Math., 4 (1970), pp. 209–223.

[42] C. Morris and H. Lecar, *Voltage oscillations in the barnacle giant muscle fiber*, Biophys. J., 35 (1981), pp. 193–213.
[43] F. Nadim, S. Zhao, L. Zhou, and A. Bose, *Inhibitory feedback promotes stability in an oscillatory network*, J. Neural Eng., 8 (2011), 065001.
[44] B. Novák and J. J. Tyson, *Design principles of biochemical oscillators*, Nat. Rev. Mol. Cell. Biol., 9 (2008), pp. 981–991.
[45] T. Nowotny and M. I. Rabinovich, *Dynamical origin of independent spiking and bursting activity in neural microcircuits*, Phys. Rev. Lett., 98 (2007), 128106.
[46] C. M. A. Pinto and M. Golubitsky, *Central pattern generators for bipedal locomotion*, J. Math. Biol., 53 (2006), pp. 474–489.
[47] R. D. Pinto, R. C. Elson, A. Szücs, M. I. Rabinovich, A. I. Selverston, and H. D. Abarbanel, *Extended dynamic clamp: Controlling up to four neurons using a single desktop computer and interface*, J. Neurosci. Methods, 108 (2001), pp. 39–48.
[48] M. Rabinovich, R. Huerta, and G. Laurent, *Neuroscience. Transient dynamics for neural processing*, Science, 321 (2008), pp. 48–50.
[49] M. I. Rabinovich, R. Huerta, P. Varona, and V. S. Afraimovich, *Transient cognitive dynamics, metastability, and decision making*, PLoS Comput. Biol., 4 (2008), e1000072.
[50] M. I. Rabinovich, P. Varona, A. I. Selverston, and H. D. I. Abarbanel, *Dynamical principles in neuroscience*, Rev. Modern Phys., 78 (2006), pp. 1213–1265.
[51] A. Rabinovitch, R. Thieberger, and M. Friedman, *Forced Bonhoeffer-Van der Pol oscillator in its excited mode*, Phys. Rev. E (3), 50 (1994), pp. 1572–1578.
[52] A. Rabinovitch and I. Rogachevskii, *Threshold, excitability and isochrones in the Bonhoeffer-Van der Pol system*, Chaos, 9 (1999), pp. 880–886.
[53] J. W. Reyn, *Generation of limit cycles from separatrix polygons in the phase plane*, in Geometrical Approaches to Differential Equations, Lecture Notes in Math. 810, Springer, New York, 1980, pp. 264–289.
[54] J. Rinzel and G. B. Ermentrout, *Analysis of neural excitability and oscillations*, in Methods in Neuronal Modeling, 2nd ed., C. Koch and I. Segev, eds., MIT Press, Cambridge, MA, 1989.
[55] J. E. Rubin, N. A. Shevtsova, G. B. Ermentrout, J. C. Smith, and I. A. Rybak, *Multiple rhythmic states in a model of the respiratory central pattern generator*, J. Neurophysiol., 101 (2009), pp. 2146–2165.
[56] M. Sammon, *Geometry of respiratory phase switching*, J. Appl. Physiol., 77 (1994), pp. 2468–2480.
[57] K. M. Shaw, M. J. Cullins, H. Lu, J. M. McManus, H. J. Chiel, and P. J. Thomas, *Evidence for a stable heteroclinic channel underlying a central pattern generator*, in 2010 Neuroscience Meeting Planner (San Diego, CA), Society for Neuroscience, 2010, online.
[58] A. Sherman and J. Rinzel, *Rhythmogenic effects of weak electrotonic coupling in neuronal models*, Proc. Natl. Acad. Sci. USA, 89 (1992), pp. 2471–2474.
[59] L. E. Spardy, S. N. Markin, N. A. Shevtsova, B. I. Prilutsky, I. A. Rybak, and J. E. Rubin, *A dynamical systems analysis of afferent control in a neuromechanical model of locomotion.* I. *Rhythm generation*, J. Neural Engrg., 8 (2011), 065003.
[60] L. E. Spardy, S. N. Markin, N. A. Shevtsova, B. I. Prilutsky, I. A. Rybak, and J. E. Rubin, *A dynamical systems analysis of afferent control in a neuromechanical model of locomotion.* II. *Phase asymmetry*, J. Neural Engrg., 8 (2011), 065004.
[61] K. M. Stiefel, J.-M. Fellous, P. J. Thomas, and T. J. Sejnowski, *Intrinsic subthreshold oscillations extend the influence of inhibitory synaptic inputs on cortical pyramidal neurons*, Eur. J. Neurosci., 31 (2010), pp. 1019–1026.
[62] K. M. Stiefel, B. S. Gutkin, and T. J. Sejnowski, *Cholinergic neuromodulation changes phase response curve shape and type in cortical pyramidal neurons*, PLoS One, 3 (2008), e3947.
[63] E. Stone and D. Armbruster, *Noise and $O(1)$ amplitude effects on heteroclinic cycles*, Chaos, 9 (1999), pp. 499–506.
[64] E. Stone and P. Holmes, *Random perturbations of heteroclinic attractors*, SIAM J. Appl. Math, 50 (1990), pp. 726–743.
[65] G. P. Sutton, E. V. Mangan, D. M. Neustadter, R. D. Beer, P. E. Crago, and H. J. Chiel, *Neural control exploits changing mechanical advantage and context dependence to generate different feeding responses in Aplysia*, Biol. Cybern., 91 (2004), pp. 333–345.

[66] G. P. Sutton, J. B. Macknin, S. S. Gartman, G. P. Sunny, R. D. Beer, P. E. Crago, D. M. Neustadter, and H. J. Chiel, *Passive hinge forces in the feeding apparatus of Aplysia aid retraction during biting but not during swallowing*, J. Comp. Physiol. A Neuroethol. Sens. Neural Behav. Physiol., 190 (2004), pp. 501–514.

[67] A. Szücs, R. Huerta, M. I. Rabinovich, and A. I. Selverston, *Robust microcircuit synchronization by inhibitory connections*, Neuron, 61 (2009), pp. 439–453.

[68] P. J. Thomas, P. H. E. Tiesinga, J.-M. Fellous, and T. J. Sejnowski, *Reliability and bifurcation in neurons driven by multiple sinusoids*, Neurocomputing, 52–54 (2003), pp. 955–961.

[69] J. V. Toups, J.-M. Fellous, P. J. Thomas, T. J. Sejnowski, and P. H. Tiesinga, *Finding the event structure of neuronal spike trains*, Neural Comput., 23 (2011), pp. 2169–2208.

[70] J. J. Tyson and B. Novak, *Regulation of the eukaryotic cell cycle: Molecular antagonism, hysteresis, and irreversible transitions*, J. Theoret. Biol., 210 (2001), pp. 249–263.

[71] A. Urban and B. Ermentrout, *Sequentially firing neurons confer flexible timing in neural pattern generators*, Phys. Rev. E (3), 83 (2011), 051914.

[72] P. L. Várkonyi, T. Kiemel, K. Hoffman, A. H. Cohen, and P. Holmes, *On the derivation and tuning of phase oscillator models for lamprey central pattern generators*, J. Comput. Neurosci., 25 (2008), pp. 245–261.

[73] P. Varona, M. I. Rabinovich, A. I. Selverston, and Y. I. Arshavsky, *Winnerless competition between sensory neurons generates chaos: A possible mechanism for molluscan hunting behavior*, Chaos, 12 (2002), pp. 672–677.

[74] H. R. Wilson, *Spikes, Decisions and Actions*, Oxford University Press, London, 1999.